MANUFACTURING, MECHANICAL AND MICROSTRUCTURAL CHARACTERIZATION OF AZ91D MAGNESIUM ALLOY FOR BIOMEDICAL APPLICATIONS

A THESIS SUBMITTED TO
THE GRADUATE SCHOOL OF NATURAL AND APPLIED SCIENCES
OF
MIDDLE EAST TECHNICAL UNIVERSITY

BY
SAİD MURAT KAYHAN

IN PARTIAL FULLFILLMENT OF THE REQUIREMENTS
FOR
THE DEGREE OF MASTER OF SCIENCE
IN
ENGINEERING SCIENCES

AUGUST 2015

Approval of thesis

MANUFACTURING, MECHANICAL AND MICROSTRUCTURAL CHARACTERIZATION OF AZ91D MAGNESIUM ALLOY FOR BIOMEDICAL APPLICATIONS

submitted by **SAİD MURAT KAYHAN** in partial fulfillment of the requirements for the degree of **Master of Science in Engineering Sciences Department, Middle East Technical University** by**,**

Prof. Dr. Gülbin Dural Ünver _____
Dean, Graduate School of **Natural and Applied Sciences**

Prof. Dr. Murat Dicleli _____
Head of Department, **Engineering Sciences**

Prof. Dr. Zafer Evis _____
Supervisor**, Engineering Sciences Dept., METU**

Prof. Dr. Muammer Koç _____
Co-Supervisor**, Sustainability Dept., HBKU, Qatar**

Examining Committee Members:

Prof. Dr. Ömer Keleş _____
Mechanical Engineering Dept., Gazi University

Prof. Dr. Zafer Evis _____
Engineering Sciences Dept., METU

Assoc. Prof. Dr. Dilek Keskin _____
Engineering Sciences Dept., METU

Assoc. Prof. Dr. Oğuzhan Yılmaz _____
Mechanical Engineering Dept., Gazi University

Assist. Prof. Dr. Erkan Konca _____
Metallurgical and Materials Eng. Dept., Atılım University

Date: 19/08/2015

I hereby declare that all information in this document has been obtained and presented in accordance with academic rules and ethical conduct. I also declare that, as required by these rules and conduct, I have fully cited and referenced all material and results that are not original to this document.

Name, Surname: Said Murat Kayhan

Signature:

ABSTRACT

MANUFACTURING, MECHANICAL AND MICROSTRUCTURAL CHARACTERIZATION OF AZ91D MAGNESIUM ALLOY FOR BIOMEDICAL APPLICATIONS

Kayhan, Said Murat

M. S., Department of Engineering Sciences

Supervisor: Prof. Dr. Zafer Evis

Co-Supervisor: Prof. Dr. Muammer Koç

August 2015, 92 Pages

In this study, the microstructural and mechanical properties of the Mg-based implant samples prepared via powder metallurgy route were investigated. Moreover, the biological response of the Mg-based implant samples was investigated. AZ91D Mg alloy discs with smooth and textured surfaces were manufactured under compaction pressures of 25 and 40 MPa at 150^{0}C. They were then sintered at 380^{0}C for 30 and 150 mins. The microstructural evaluation was conducted through SEM and light microcopy images. As compaction pressure increased, the relative densities of the discs increased (0.57-0.67%) as well as the diametral tensile strength (2.55-3.01 MPa) and Vickers micro-hardness values (13.5-84.1 HV2). Extended sintering time did not affect the relative densities while increased the hardness of the discs. It was also found that sintering time did not affect significantly the diametral tensile strength. However, the discs with textured surface had lower relative density. The sintered discs had higher mechanical and relative density values than the unsintered ones. The validity of relative density measurements was provided by image processing technique and finite element method. The Mg alloy discs showed no toxicity in methylthiazolyldiphenyl-tetrazolium (MTT) assay. It was also seen that

the discs with a textured surface with channels had more cell viability than the disc with a smooth surface.

Keywords: AZ91D magnesium alloy, Powder metallurgy, Microstructural evaluation, Mechanical characterization, MTT assay.

ÖZ

BİYOMEDİKAL UYGULAMALAR İÇİN AZ91D MAGNEZYUM ALAŞIMININ İMALATI, MEKANİK VE MİKROYAPISAL KARAKTERİZASYONU

Kayhan, Said Murat
Yüksek Lisans, Mühendislik Billimleri Bölümü
Tez Yöneticisi: Prof. Dr. Zafer Evis
Ortak Tez Yöneticisi: Prof. Dr. Muammer Koç
Ağustos 2015, 92 Sayfa

Bu çalışmada, toz metalurjisi yoluyla hazırlanmış Mg-tabanlı implant numunelerin mikroyapısal ve mekanik özellikleri incelenmiştir. Bununla birlikte Mg tabanlı implant örneklerinin biyolojik özellikleri de araştırılmıştır. Düz ve şekilli yüzeye sahip AZ91D Mg alaşımı diskleri 25 ve 40 MPa basınçlar altında ve 150^{0}C sıcaklıkta üretilmiştir. Daha sonra 380^{0}C sıcaklıkta 30 ve 150 dakika boyunca sinterlenmişlerdir. SEM ve ışık mikroskobu görüntüleri üzerinden mikroyapısal değerlendirmeler yapılmıştır. Sıkıştırma basıncı arttıkça disklerin bağıl yoğunluk değerlerinin (0.57-0.67%) yanı sıra çapsal çekme mukavemeti (2.55-3.01 MPa) ve Vickers mikro sertlik değerleri (13.5-84.1 HV2) de artmıştır. Uzun sinterleme süresi disklerin bağıl yoğunluk değerlerini etkilemezken disklerin sertliğini arttırmıştır. Ayrıca, sinterlemenin çapsal çekme dayanımına belirgin bir etkisinin olmadığı bulunmuştur. Ancak, yüzey şekilli diskler düşük bağıl yoğunluğa sahiptirler. Sinterlenmiş diskler, sinterlenmemiş olanlara gore daha yüksek mekanik dayanıma ve bağıl yoğunluk değerlerine sahiptirler. Bağıl yoğunluk ölçümlerinin doğruluğu görüntü işleme ve sonlu elemanlar yöntemi ile sağlanmıştır. Mg alaşımı diskleri MTT testinde hiçbir toksik özellik göstermemiştir. Ayrıca, kanallı yüzey şekillerine

sahip olan Mg diskler yüzey şekline sahip olmayana göre daha yüksek bir canlılık oranına sahip olduğu görülmüştür.
Anahtar Kelimeler: AZ91D magnezyum alaşımı, Toz metalurjisi, İç yapı özellikleri, Mekanik özellikleri, MTT testi

ACKNOWLEDGMENTS

I would like to express my deepest gratitude to my advisor, Prof. Dr. Zafer Evis, for his excellent guidance, caring, patience, and providing me with an excellent atmosphere for doing research. I am also so grateful to Prof. Dr. Muammer Koç for encouraging me in this fascinating field and for letting me benefit from his profound mind and knowledge.

I owe my thanks to Assoc. Prof. Dr. Ayşen Tezcaner and Assoc. Prof. Dr. Dilek Keskin for their generosities to let me work in their Biomaterials laboratory. I also thank to Assoc. Prof. Dr. Yusuf Usta for their guidance in the manufacturing step.

I would like to thank Aydin Tahmasebifar, who as a good friend was always willing to help and give his best suggestions. It would have been a lonely lab without him. I also would like to thank my other dear lab friends; Engin Pazarçeviren, Deniz Atila, Ali Deniz Dalgıç, Alişan Kayabölen, Reza Moonesirad, Sibel Ataol and Hazal Aydoğdu for their support.

I would like to thank to The Scientific and Technological Research Council of Turkey for the financial support to this study (Project no: 112M340).

I would like to give my greatest thanks to my parents, Erol Kayhan and Fatma Kayhan, and my sisters, Nurdan Kayhan and Ayşenur Kayhan, for the values they taught and the endless support they provided through my entire life. Their respect and belief in what I do is precious for me.

I also place on record, my sense of gratitude to one and all who, directly and indirectly, have lent their helping hand in this venture.

TABLE OF CONTENTS

LIST OF FIGURES

FIGURES

LIST OF TABLES

TABLES

CHAPTER 1

INTRODUCTION

1.1 Biomaterials

Biomaterials are classified into three important terms according to their behaviors in a biological environment. These are bioinert, bioactive and reabsorbable biomaterials. Bioinert materials do not interact with any biological system and release any toxic substance while bioactive materials interact with biological system and help to biological system to recover. Reabsorbable biomaterials can degrade within a living system without any negative effect. There are four types of biomaterials clinically used can be listed as (1) metals (2) ceramics, (3) polymers and (4) composites (Bartolo et al., 2012).

1.1.1 Metals

The most used material type in biomedical applications is metals and their alloys, which are also called as metallic biomaterials. Stainless steels, titanium alloys and cobalt-chromium alloys have been used as biomaterials in clinical applications (Table 1). Except from these, other metallic biomaterials are iron (Fe), tantalum (Ta), niobium (Nb) and magnesium (Mg) alloys and so on but their clinical applications are limited (Niinomi et al., 2012). Metallic biomaterials are generally used in bones (fractured or age-related non-functional) because of their superior mechanical properties including high strength, ductility, toughness, fatigue life etc., which are extremely important for load bearing applications such as hip and knee joints (Niinomi, 2007; Ren and Yang, 2013). Its relatively low cost is another advantage of metallic biomaterials (Ferreira et al., 2003). Besides their superiorities, there are some limitations on the use of metallic biomaterials in a biological environment. Metals are actually bioinert materials and they do not release any toxic ions in normal conditions (Table 2). However, in case of corrosion or wear arising from

impurities or defects, metallic ions may cause a toxic effect in the living organisms. Additionally, metallic biomaterials do not show similar elastic behavior when compared to natural bone and this causes negative effect on mechanical integrity of biomaterials (i.e. implant loosening due to elastic mismatches) and the living environment (Staiger et al., 2006).

Table 1. Biomaterials and applications (Bauer et al., 2013).

	Biomaterials	Applications
Metals	Cobalt–chromium alloys Stainless steel Titanium alloys	Artificial heart valves, dental prosthesis and implants, orthopedic fixation plates and screws, artificial joint components, vascular stents, vascular stents, artificial joint components, pacemaker cases
Ceramics	Aluminum oxides Zirconium oxides Calcium phosphates Bioactive glasses	Orthopedic joint replacement, orthopedic load-bearing implants, dental implants, Orthopedic and dental implant coatings, dental implant materials, bone graft substitute materials
Polymers	Many polymers derived synthetically and naturally	Orthopedic applications, syringes, heart valves, sutures, breast implants, contact lenses, heart valves, artificial hearts vascular grafts, sutures, bone cements, dental implants, pharmaceutical fillers, urinary bladder catheter, vascular grafts, resorbable meshes, drug delivery devices

1.1.2 Ceramics

Ceramics are generally known as brittle inorganic materials with high compressive strength and bioinertness but lower tensile strength than metals (Bartolo et al., 2012; Holzapfel et al., 2013). They also have higher elastic modulus when compared to bone (Holzapfel et al., 2013). The most frequently used ceramic biomaterials are metallic oxides, calcium phosphate (mostly known as hydroxyapatite) (Bartolo et al., 2012). Metallic oxides are bioinert materials that have high mechanical strength, high wear and corrosion resistance and biocompatibility (Bartolo et al., 2012). Owing to high mechanical strength of metallic oxides such as Al_2O_3 and MgO, they are generally used in high load bearing implants (i.e. hip implants). However, calcium phosphates may interact with biological system when the material is implanted. And calcium phosphates are not applicable due to their poor mechanical properties in applications requiring high strength (Rosengren et al., 2002).

1.1.3 Polymers

Polymeric biomaterials are classified as natural and synthetic material as well as biodegradable and bioinert (Table 2). In clinical applications, there are so many different types of synthetic/natural or biodegradable/bioinert polymeric biomaterials. Polymers such as polyvinyl chloride (PVC), polyethylene (PE), polypropylene (PP), polymethylmethacrylate (PMMA), polystyrene (PS), polytetrafluoroethylene (PTFE), polyesters, polyamides (PA-nylon), polyurethanes (PUR), and polysiloxanes (silicone) have used in biostable synthetic applications. Glycolic acids, lactic acids, their copolymers, and p-dioxanone are the examples of biodegradable synthetic polymers. There are also numerous natural polymer including dextran, silk, heparin, DNA and the others. The applications of polymeric biomaterials are various such as drug delivery, fixation devices for orthopedics and scaffolds for tissue engineering (Bartolo et al., 2012; Holzapfel et al., 2013).

Table 2. Behavioral analysis of biomaterials in a biological system (Holzapfel et al., 2013).

	Inert	Active	Reabsorbable
Metals	✓	✗	✗
Ceramics	✓	✓	✓
Polymers	✓	✗	✓

1.1.4 Composites

Composites are another type of biomaterials that are not used frequently. Most composite biomaterials are polymer based materials in the applications. As it is known, composites compose of a matrix and reinforcement. Reinforcements can be vital (living) or avital (non-living) while matrices can be only avital so that composites are called avital/avital and vital/avital (Bartolo et al., 2012).

1.2 Biomedical Implants

The first definition of biomedical implants was reported in 1986 by the European Society for Biomaterials as "any medical device made from one or more materials that is intentionally placed within the body, either totally or partially buried beneath an epithelial surface". An implant differs from other medical equipment because they are used especially for replacing organ or tissue totally or partially (Bauer et al., 2013). However, implants are used to assist or enhance the functioning of biological systems additional to replacing (Bartolo et al., 2012). Material types used in manufacturing of biomedical implants are discussed in previous section. The intended use of implants can be either clinical or non-clinical. They are also used permanently or temporarily in the body. The schematic representations of biomedical implants which are classified according to their intended use are shown in Figure 1.

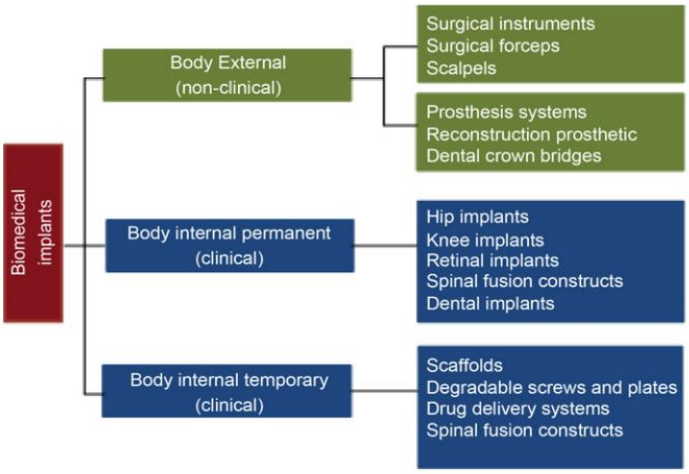

Figure 1. Classification of biomedical implants (Bartolo et al., 2012).

A biomedical implant has general requirements that have to be satisfied during its life cycle. These general requirements are compatibility, functionality, durability and safety that are so important for the functioning of an implant (Niinomi et al., 2012). Specifically speaking, all implants should have two main properties including 1) mechanical sufficiency and 2) compatibility and environmental stability. Having appropriate mechanical properties (i.e. strength and elastic modulus) is an important issue for durability and safety of implants because the role of an implant is to support physically the damaged tissue during healing process. An implant is also expected to have sufficient strength (tensile or compressive) in orthopedic applications. For instance, an enormous difference between elasticity's of implant and damaged bone may lead elastic mismatches and causes stress shielding in especially metallic biomaterials which are used for orthopedic applications. A schematic representation is shown in Figure 2. Metallic materials (100-200 GPa) are generally stiffer than bone (1-20 GPa) and this inequality causes that a major part of stresses is carried by the implant. The unbalanced stress between the material and the bone makes the bone softer and blocks the healing of the bone in addition to failure due to excessive loading on the implant (Haase and Rouhi, 2013). In order to remove stress shielding, metal implants such as Ti and alloys were manufactured with pores by powder metallurgy technique and their elastic modulus is reduced to level of 40 GPa which is

very close to that of natural bone (≈20 GPa) (Haugen et al., 2013; Hsu et al., 2014; Omidi and Bahmani Oskooee, 2013; Tan et al., 2013). During healing process, another important necessity is that an implant has to be compatible and environmentally stable. One hand, implant materials should not show any toxic or allergenic reaction or they have to stay in reasonable levels. On the other hand, they should have excellent corrosion and wear resistance.

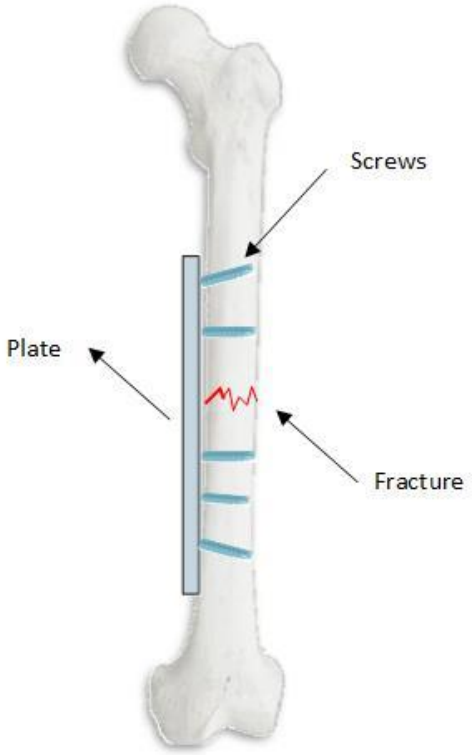

Figure 2. A bone-implant system.

1.2.1 Biodegradable implants

Biodegradable implants have emerged as an excellent alternative to conventional non-degradable implants, which are used permanently in a living system. They are generally manufactured by metals, ceramics and polymers (Salahshoor and Guo, 2011; Tan et al., 2013). The working principle of biodegradable implants, which is based on corrosion, in a biological system can be explained basically as follow: (1)

Implantation, (2) Supporting and assisting to bone during healing and (3) Corroding into living system after healing process (Ren and Yang, 2013). Biodegradable implants subordinate to conventional implants in many ways. The most challenging part of implantation is surgery in terms of cost and time. While permanent biomedical implants need two surgical interventions (the first one is for inserting, the second one is for de-inserting), biodegradable implants remove the second surgical intervention by degradation of implant. Thus, biodegradable implants offer a great opportunity to reduce cost and time consuming by preventing second surgical operation. The increase in the number of surgical operations also increases the risk of life in patients. Moreover, it causes a reduction in work-force of the country additional to the lack of social life. However, corrosion mechanism needs to be argued intensively because excessive corrosion rate could bring the lack of mechanical support before healing is not completed. Therefore, an optimization is needed on corrosion rate of biodegradable implants. Relationship between corrosion and implantation time is shown graphically below (Figure 3).

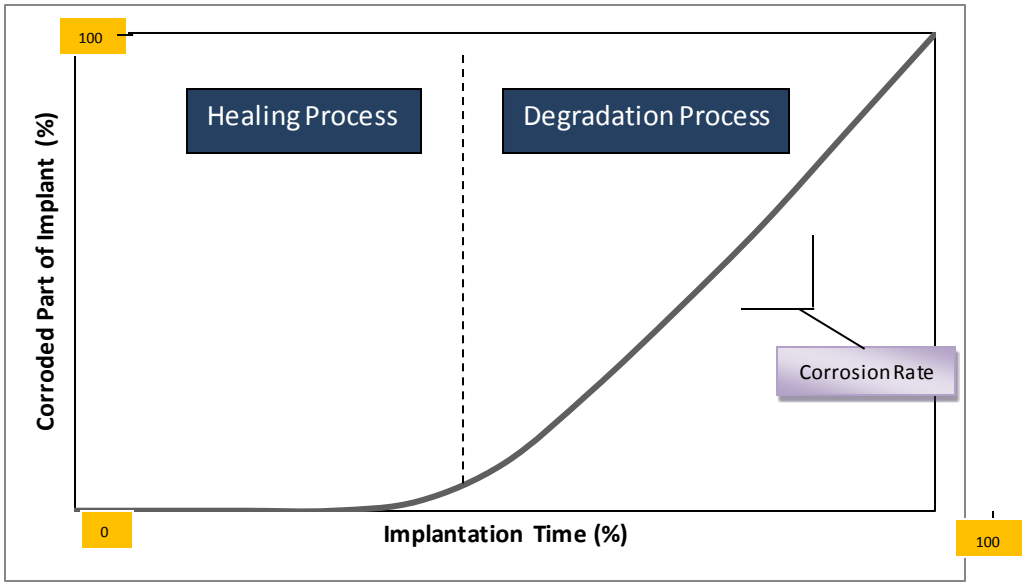

Figure 3. The relationship between corrosion and implantation time in biodegradable implants.

Biocompatibility and biodegradability are very critical and versatile terms for evaluating the success of temporary implants. Biocompatibility covers three basic

prerequisites: (1) Implanted material needs to be accepted by host tissues, (2) It should not show any toxic, allergenic, immunogenic, carcinogenic effect etc. and (3) should not show any unexpected corrosion profile which causes chemical unstabilization in biological system (Ringoir and Vanholder, 1986). Biodegradable implants are based on degradation capability of the implant. Thus, biodegradability is highly related to corrosion behavior of an implant. Biodegradability is the ability that measures level of dissolution of an implant into non-toxic corrosion products. These two terms are affected by many parameters during implantation time. The effective parameters can be named as (1) material type, (2) surface condition, (3) manufacturing method and (4) interaction level with biological environment.

Materials which are used as biodegradable implants are limited as stated before. Nevertheless, biodegradable implant materials exhibit different physical and chemical behaviors in different environments and these affect degradation profile of an implant (Table 2). This shows that material selection is an important issue in terms of biocompatibility and biodegradability.

Another important property is surface condition of the implant. Micro and nano-features on implant surface may change surface characteristics such as roughness. Roughness or surface structures on an implant surface are critical for cell adhesion and proliferation. However, optimum aspect ratio of these structures needs to be taken into consideration. One hand, cells cannot reach oxygen and live on surface structures with low aspect ratio. On the other hand, high aspect ratio may not be enough for the attachment of cells on the surface. In a study, it was observed that cell attachment and proliferation are much more on micro-grooved implant surface with the dimension of 10 and 120 μm (Fu and Soboyejo, 2009). Porosity on the implant surface also makes a major contribution to bone-implant integration by increasing cell attachment (Brånemark et al., 2011; Fu and Soboyejo, 2009; Mirhosseini et al., 2007). Micro and nano-surface structures not only increase the compatibility of implants but also improve corrosion resistance (Wu et al., 2013). In another word, surface characteristics have great influence on corrosion. Such changes affect corrosion behavior of the implant eventually.

Defects such as contamination that come from manufacturing process may have possible health risks. The rate of contamination depends on manufacturing methods as well as manufacturing conditions. For instance, casting is so prone to contamination so sterilization should be applied.

Biological systems can act in different manners in a foreign body such as implant even if an implant has the same conditions/properties in each implantation due to their complex and unforeseen reactions. To design biodegradable and biocompatible implants, the interactions between implant and biological environment should be well defined as in other prerequisites.

1.2.1.1 Magnesium and its alloys

Magnesium is an ultra-light material among other metallic materials having a density of 1.74 g/cm^3 (Duan et al., 2014). Magnesium and its alloys are applicable in many industries including automotive, aerospace, electronic devices etc. due to their high specific strength in addition to their lightness (Staišiūnas et al., 2014). The need for lightness is increasing in terms of energy efficiency. Advantages of magnesium can be augmented. Magnesium has good machinability and dimensional stability. It can preserve material properties when used in electrical processes (Chu et al., 2014). Its recyclability increases the number of industrial applications (Fan et al., 2014). However, magnesium and its alloys have some deficiencies in thermal and chemical processes. Working temperature is high and electrical conductivity should be low in thermal processes such as conventional welding methods. Weldability of magnesium and its alloys is limited because of their high thermal and electrical conductivity (Duan et al., 2014). Magnesium based materials also have low chemical stability and corrosion resistance that lead to infirmities in mechanical and physical properties of materials (Chu et al., 2014). These thermal and physical deficiencies hinder extensive use of magnesium and its alloys in the industry.

Magnesium-based materials as biodegradable implants have many advantages over conventional ones. Their degradability within human, non-toxicity, non-allergenicity and preventing second surgical operations was mentioned previously as advantages of biodegradable implants. Apart from these, magnesium and its alloys have

mechanical properties which are fairly close to human bone when compared to other metallic implants. For instance, according to Table 3, magnesium alloys have closer Young's modulus (40-45 GPa) to human bone (3-23 GPa) than other metallic implants such as Ti alloys (100-117 GPa), Co-Cr alloys (210-232 GPa) and stainless steel (189-205 GPa). This similarity reduces the difference between the implant and bone elastic moduli and lowers the extent of stress shielding effect. Additionally, magnesium alloys have the most suitable strength properties (yield, tensile and compressive) for human bone as seen in Table 3. The other superior property of magnesium is that its corrosion products are not harmful for human. On the contrary, lack of magnesium ions in the human body may cause diseases in human bone (osteoporosis) because it is a base element for bones (Bauer et al., 2013). It was also reported as an osteoconductive material (Willumeit et al., 2011) and accelerates osteointegration (Castellani et al., 2011). Owing to its positive osteogenic properties, it can be said that using magnesium alloys as biodegradable implants reduces healing time by assisting to healing process and formation of damaged bone.

The first use of magnesium in human as biomaterial has been started in the beginning of 19th century (Witte, 2010). In the beginning stages of using magnesium, only pure magnesium was used and it was understood that pure magnesium has very low corrosion resistance in aggressive chloric environments such as blood. Pure magnesium has been manufactured as sheets, plates, screws, wires etc. and investigated for nearly 100 years in human and many animals (pigs, dogs, rats, cats, rabbits) (Witte, 2010). In some applications, magnesium was alloyed with metals including aluminum (Al), cadmium (Cd), manganese (Mn) but was very few in number (Witte, 2010). However, investigations on magnesium as biomaterials diminished rapidly due to fast corrosion of pure magnesium in chloride environment such as body fluid (103.0 $mmol^{-1}$) (Bauer et al., 2013; Witte, 2010).

Table 3. Comparative representation of human bone and metallic biomaterials in terms of material properties.

Material Property	Human Bone	Mg Alloys	Ti Alloys	Co-Cr Alloys	Stainless Steels
Density (g/cm^3)	1.8-2.1	1.74-2.00	4.4-4.5	8.3-9.2	7.9-8.1
Yield Strength (MPa)	30-114.3	20-200	896-1034	448-1606	221-1213
Compressive Strength (MPa)	164-240	55-130	N/A	N/A	N/A
Young's Modulus (GPa)	3-23	41-45	110-117	210-232	189-205
Tensile Strength (MPa)	70-150	86-280	760-1140	655-1896	586-1351
Elongation (%)	1.07-2.10	12-21	12	N/A	N/A
Data compiled from references (Bauer et al., 2013; Gu and Zheng, 2010; Moravej and Mantovani, 2011; Sun et al., 2012; Zhang et al., 2013b)					

With the emerge of biodegradable implant concept, magnesium and its alloy have started to be investigated by researches again in the late of 90's. Corrosion is not considered entirely as a problem anymore but it has turned into a process need to be controlled. Two compounds (magnesium hydroxide and hydrogen gas) develop as corrosion product of magnesium when it exposes to body fluid. Corrosion products are described in a general chemical reaction equation as follow (Dorozhkin, 2014).

$$Mg_{(s)} + 2\ H_2O_{(aq)} \leftrightarrow Mg(OH)_{2\ (s)} + H_{2\ (g)} \quad (1)$$

But general reaction is formed from three incomplete reactions:

$$Mg_{(s)} \leftrightarrow Mg^{2+}_{(aq)} + 2\ e^{-}\ \text{(anodic reaction)} \quad (2)$$

$$2\ H_2O_{(aq)} + 2\ e^- \leftrightarrow H_{2\ (g)} + 2\ OH^-_{(aq)} \text{ (cathodic reaction)} \quad (3)$$

$$Mg^{2+}_{(aq)} + 2\ OH^-_{(aq)} \leftrightarrow Mg(OH)_{2\ (s)} \text{ (product formation)} \quad (4)$$

There are four types of corrosion which may dominate during healing process. Galvanic corrosion, pitting corrosion, erosion corrosion and corrosion fatigue are forms of corrosion which may occur in the human body fluid (Bauer et al., 2013). The reasons of corrosion can be several such as alloying elements, microstructure, manufacturing process, heat treatment and so on (Bauer et al., 2013).

Many methods have been offered to enhance corrosion resistance of pure magnesium. Alloying and subsequent treatments (heat or chemical) are options to prevent rapid degradation of pure magnesium. As expected, alloying metal should also be compatible for human body just as implant materials. Ca, Zn and Mn are known as harmless materials to living systems. It is also known that a trace of rare earth elements (REE) can be allowed within the body (Hermawan et al., 2010). Many metals were alloyed with pure magnesium in order to obtain suitable degradation profile for a biodegradable implant. A classification was made (Willumeit et al., 2011) into four types of alloying system as listed: (1) AZ - aluminum and zinc, (2) AM - aluminum and manganese, (3) WE - yttrium and REE and (4) LAE - lithium, aluminum and REE. Magnesium alloys are mostly investigated within this framework. Corrosion behaviors of four different magnesium alloys (AZ31, AZ91, WE43 and LAE442) were investigated in vivo (Witte et al., 2005). LAE442 had the slowest degradation rate. As a result, it was reported that alloying reduces fast degradation of magnesium. AZ31 magnesium alloy was studied both in vivo and vitro (Song et al., 2009; Willbold et al., 2011). Corrosion behavior of AZ31 was investigated by inserting screws in sheep bone. AZ31 was also immersed in simulated body fluid (SBF) for 2h, 6h, 12h, 24h and 48h at 37°C. Studies showed that the surrounding environment has great influence on corrosion behavior of AZ31 bone screws. In another study (Geis-Gerstorfer et al., 2011), eight different Mn-free magnesium alloys including MgZn1 (Z1), MgAl3 (A3), MgAl9 (A9), MgNd2 (E2), MgY4 (W4), MgAl3Zn1 (AZ31), MgAl9Zn1 (AZ91) and MgY4Nd2 (WE43) were investigated both in human blood and in SBF. The results differ from in human blood

and in SBF proved that the surrounding environment is critical for corrosion. MgAl9 and MgAl9Zn1 had slow degradation rates in human blood. REE's were used (Yang et al., 2011) to decrease corrosion rate of magnesium. Corrosion of binary Mg-Dy alloys with different dysprosium (Dy) content after heat treatment (T4) were characterized by immersion test. Hydrogen gas (H_2) evaluation showed that the increase in the content of Dy improved corrosion resistance of the binary alloy. T4 treatment also decreased corrosion rate by making more homogenous the structure of Mg-Dy binary alloy when compared as-cast Mg-Dy binary alloy. Magnesium was alloyed (Hort et al., 2010) with different Gadolinium (Gd) contents (2, 5, 10 and 15 wt.%) as the same in previous work. Mg-Gd binary alloy was exposed to T4 (solutionizing) and T6 (ageing) heat treatments and compared with normal condition (as-cast). Corrosion rate decreases as the content of Gd is increased. However, Mg-Gd binary alloy with the content of 15 wt.% corroded slightly. It was also stated that the heat treated materials showed better corrosion resistance over the as-cast binary alloy. Extruded LAE442 magnesium alloy (Witte et al., 2010) was evaluated in white rabbits in terms of corrosion resistance and corrosion rate founded at acceptable level.

Surface modification such as coating is another option to reduce rapid corrosion rate of magnesium. Many trials on coating of magnesium alloys have been done both in vivo and in vitro. Calcium-phosphate based materials are frequently used for coating material because they are good biocompatible materials and have positive effect on the bone (Hornberger et al., 2012). Both in vivo and in vitro studies showed (Lu et al., 2014; Xiao et al., 2013; Xu et al., 2009) that porous Ca-P coatings on magnesium and its alloys including Mg–Mn–Zn (Mg–1.2 Mn–1.0 Zn, in wt.%), AZ60 and 99.99% pure magnesium reduce significantly corrosion rate as well as increasing bioactivity between bones and implants. Hydroxyapatite (a type of Ca-P) coating was achieved on AZ91 magnesium alloys by sol-gel method and electrophoretic deposition in two different studies (Rojaee et al., 2013). In both studies, it was observed that surface of the materials did not corrode excessively. Also, surfaces were active in bone formation because hydroxyapatite is the most weighted composition of bone. Polymeric material coatings from different organic materials exist in the literature (Hornberger et al., 2012). An important study was conducted

(Wong et al., 2010) that AZ91 magnesium alloy was coated by a biodegradable polymer-based material (polycaprolactone (PCL) + polycaprolactone (PCL)) and observed its corrosion resistance and contribution to new bone formation. The results showed that the corrosion resistance and new bone formation increase significantly.

1.2.1.2 Mg-based foams

Low strength Mg and its alloy foams have been proposed for bone reconstruction and regeneration due to their high specific strength and absorbance capacity per volume (Aghion and Perez, 2014). They also have been used in tissue engineering and drug delivery systems as well as non-biomedical areas such as transportation (Li and Zheng, 2013). Mg-based scaffolds came to the forefront owing to the fact that their counterparts including specific polymers, poly(-hydroxyesters) and hydroxyapatite have low mechanical stability, elasticity and ductility (Aghion and Perez, 2014). Their porosity levels were ranged from 25-55 % (Li and Zheng, 2013). Porous degradable Mg-based scaffolds had pore size of 73-500 micron while their elastic moduli were measured in between 0.41 and 1.8 GPa (Li and Zheng, 2013). Several methods have been proposed for manufacturing Mg-based scaffolds with excessive porosity (Li and Zheng, 2013). PM was one of them due to its high ability to manufacture porous materials. Witte et al. were able to manufacture AZ91D magnesium alloy foam having porosity of 72-76 % and pore size of 10-1000 μm (Witte et al., 2007). The magnesium alloy scaffolds showed excellent biocompatibility and inflammatory response in vivo. Wen et al. produced via PM route highly porous Mg pellets with 50% porosity and 200-500 μm (Wen et al., 2004). The strength of scaffold was 2.33 MPa in compression test which was very close to cancellous human bone (3-20 MPa) (Li and Zheng, 2013). However, the elastic modulus (0.35 GPa) was relatively low compared to natural bone (10-40 GPa) due to high porosity. Xia et al. have also proved that the yield strength of AZ31 magnesium alloy scaffolds decreased as porosity increased from 60 to 75% when pore size increased at the same time (Xia et al., 2013). Pure Mg scaffolds with controlled (patterned) structure were manufactured but biological and mechanical properties were not well established (Staiger et al., 2010). Mg-based foams and scaffolds are represented in Figure 4.

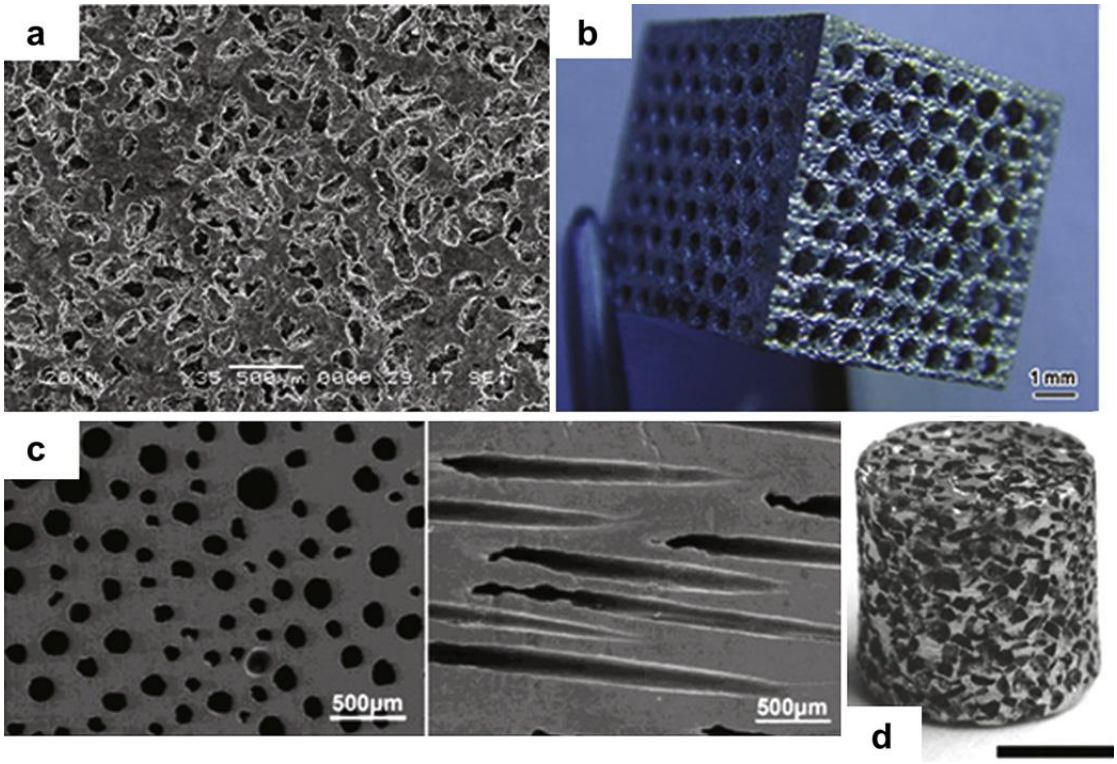

Figure 4. Configuration of porous magnesium scaffold prepared by powder metallurgy (a) and other techniques (b,c,d) (Li and Zheng, 2013).

1.2.1.3 AZ91D magnesium alloy

AZ91D is one of the alloy systems, which is used in biomedical applications. It has hexagonal closed packed crystal structure with low density (Yan et al., 2014). AZ91D mainly consists of Al and Zn as alloying elements in its composition (Willumeit et al., 2011). Trace amount of Si, Cu, Be and Ni exist in the composition but they do not have any significant effect on the material properties (Yan et al., 2014). Al and Zn are major alloying elements for Mg based alloys (Virtanen, 2012). The effect of Al and Zn in AZ91D magnesium alloy causes strengthening by possessing microstructural development. Small amount of secondary dendritic phase ($Mg_{12}Al_{17}$) increases the mechanical performance of the magnesium alloy. However, redundant dendritic phase in the composition may result in a sharp decrease in the mechanical properties (Yan et al., 2014).

Al is used to alloy with Mg due to its high solubility limit and improved mechanical properties (Chen et al., 2014). Although excessive amount of Al may have toxic effect in the human body, it has a substantial impact on the mechanical properties (Bakhsheshi-Rad et al., 2014). Al is mainly responsible for enhancing mechanical strength of the magnesium alloy as well as decreasing degradation rate in vivo (Purnama et al., 2014). One problem with Al as alloying material is the risk of secondary phase formation that hampers grain boundaries (Homayun and Afshar, 2014). This causes the lack of mechanical properties such as hardness, elastic modulus, tensile and compressive strength. Excessive amount of Al has been stated as a secondary phase former ($Mg_{12}Al_{17}$) in the presence of Ca (Homayun and Afshar, 2014). Mg has hexagonal and $Mg_{12}Al_{17}$ has cubic crystal structure (Liu et al., 2014).

Zn is one of the nutrition elements in the human body with high solubility (6.2 wt.%) in Mg and moderate daily intake (15 mg/d) dosage (Chen et al., 2014). Zn is also a main constituent for more than 200 biological assets (Du et al., 2011). On the other hand, it has been found that Zn is also related to particular cancers (Narayanan et al., 2014). Zn addition improves mechanical properties of Mg alloys. However, Zn has stronger impact on the mechanical properties when Zn content is small (Zhang et al., 2012). Microstructure and mechanical properties are two outputs in bulk materials, which have reciprocal relationship. A microstructure with homogeneous and small grains is expected to have improved mechanical properties (Gzyl et al., 2015). Grain refinement, solid solution or precipitation strengthening could be the reason for improved mechanical properties of Zn-doped Mg alloys (Brar et al., 2012). Intermetallic phase in Mg-Zn system (MgZn) precipitates at grain boundaries and with the addition of Zn, grain size decreases (Zhang et al., 2013a). High Zn content increases the hardness, elongation capability, tensile and compressive strength of these alloys (Brar et al., 2012; Du et al., 2011; Peng et al., 2012). Presence of other elements (Ca and Sr) also did not affect the increasing effect of Zn content (Brar et al., 2012; Du et al., 2011). Zn addition results in thinner grain boundaries and refined grain size. A study has proved that increase in Zn content from 4 to 6 wt.% caused a decrease in grain size of the alloy (Seyedraoufi and Mirdamadi, 2013). It has also been reported that secondary phase formation in the alloy contributed mechanical improvement even if elongation capability of the alloy was restricted (Du et al.,

2011). Mn has also improved tensile strength and elongation of the magnesium alloy in the presence of Zn (Zhang et al., 2009). The effect of Si is similar to Al due to their ability to form intermetallic compounds (Mg_2Si and $Mg_{17}Al_{12}$, respectively). In a Mg-Al-Zn alloy system, it has been reported that Si intermetallic phase was formed and it did not affect the formation of Al intermetallic phase (Mazraeshahi et al., 2015). Addition of Si at moderate level has contributed an increase in hardness by allowing Mg_2Si dendritic phase formation according to another study (Srinivasan et al., 2010). Thus, trace amount of Si addition as in AZ91D magnesium alloy results in microstructural refinement and improve mechanical performance but redundant Si may cause brittle fracture (Srinivasan et al., 2010).

1.2.2 Implant manufacturing methods

Both conventional (i.e. casting, machining, molding and plastic deformation) and non-conventional (Chemical Vapor Deposition (CVD), Physical Vapor Deposition (PVD) and so on) methods have been used in manufacturing of biomedical implants (Denkena and Lucas, 2007; Guo and Salahshoor, 2010; Harandi et al., 2011; Kaiser et al., 2013; Klocke et al., 2013; Maru et al., 2015; Okulov et al., 2013; Palanivelu et al., 2014; Rothen-Weinhold et al., 1999). Almost in every implant, two or more manufacturing methods are used as combined in order to get multi-function products in applications.

Many implants have been manufactured by casting and secondary manufacturing operations such as coating applications, extrusion, machining etc. The methods have been applied to investigate the effect of manufacturing methods on the functioning of implants. In a study (Kaiser et al., 2013), a Co alloy was prepared to analyze the effect of cooling rate in casting on the mechanical properties. Mechanical properties of Co alloy were characterized by the hardness and tensile test. It was concluded that the increase in the cooling rate decreases the ductility but increases the strength of the specimens. This also increases in the hardness values. The same study (Okulov et al., 2013) was conducted on a Ti alloy and showed that the formation of microstructure during casting affects profoundly the mechanical properties of the specimens.

The first contact between implant and bone occurs on their surfaces and thus surface properties have great importance on corrosion and mechanical behavior of an implant. However, machining as a manufacturing technique may break surface integrity that is necessary for proper functioning of implants. In many studies, the effect of machining process on implant properties was investigated. Mg-Ca alloy (Guo and Salahshoor, 2010) was machined at high cutting speed without using any lubricant and observed surface characteristics including surface roughness, residual stress on the surface, surface microstructure and micro-hardness. Also, the machining process was simulated by using Abaqus in 2D with the purpose of making comparison between actual machining and simulation. Surface integrity was preserved with smooth roughness at high cutting speed. High residual stresses and micro-hardness were measured on the specimen surfaces with high cutting speed. Residual stresses and chip formation was well-estimated by simulation. In another study (Denkena and Lucas, 2007), the relationship between surface properties and corrosion was studied on the machined Mg-Ca alloy. It was found that surface properties coming from machining have great influence on corrosion. The effect of electrical discharge machining (EDM) on biocompatibility of WE43 magnesium alloy was investigated (Klocke et al., 2013) by cutting stainless steel (SS) wire. For understanding the thermal effect of EDM on toxicity, three different cutting conditions (fine to rough cut) were applied. In rough cut, contamination was detected in toxicity tests and reduced the absorption rate of magnesium alloy.

Plastic deformation is one of the most preferred manufacturing techniques owing to not having waste material during process. Implants have been manufactured by plastic deformation for better understanding its applicability in the literature. Forging was used (Harandi et al., 2011) to manufacture Mg-1Ca biodegradable magnesium alloy at different temperatures and forging speeds and to evaluate its mechanical and corrosion properties. Hardness values were directly proportional until a specific temperature and forging speed and after reaching maximum hardness value it became inversely proportional. This shows that there is an optimization point on hardness depending on temperature and forging speed. A comparative study (Rothen-Weinhold et al., 1999) was made between extrusion and injection molding for the feasibility of manufacturing of biodegradable implants. It was stated that

manufacturing biodegradable implant with both methods is feasible but injection molding technique is more suitable to manufacture for complex parts.

1.3 Powder metallurgy

Powder metallurgy (PM) is one of the oldest manufacturing methods that is used to manufacture either porous or non-porous products from powders. It is also a common manufacturing technique because it enables higher tolerances with low cost over other techniques (Smith et al., 1998). Although its history is based on old times, it is widely used in many fields of modern industry. The scope of PM covers some medical applications, porous metals, self-lubricating machine parts, automotive components etc. (Smith et al., 1998). PM is the most suitable manufacturing method especially for porous parts. PM consists of several steps starting form fabrication and characterization of powder, following compaction and sintering and ending with final net shaping. General scheme of PM processes is presented in Figure 5.

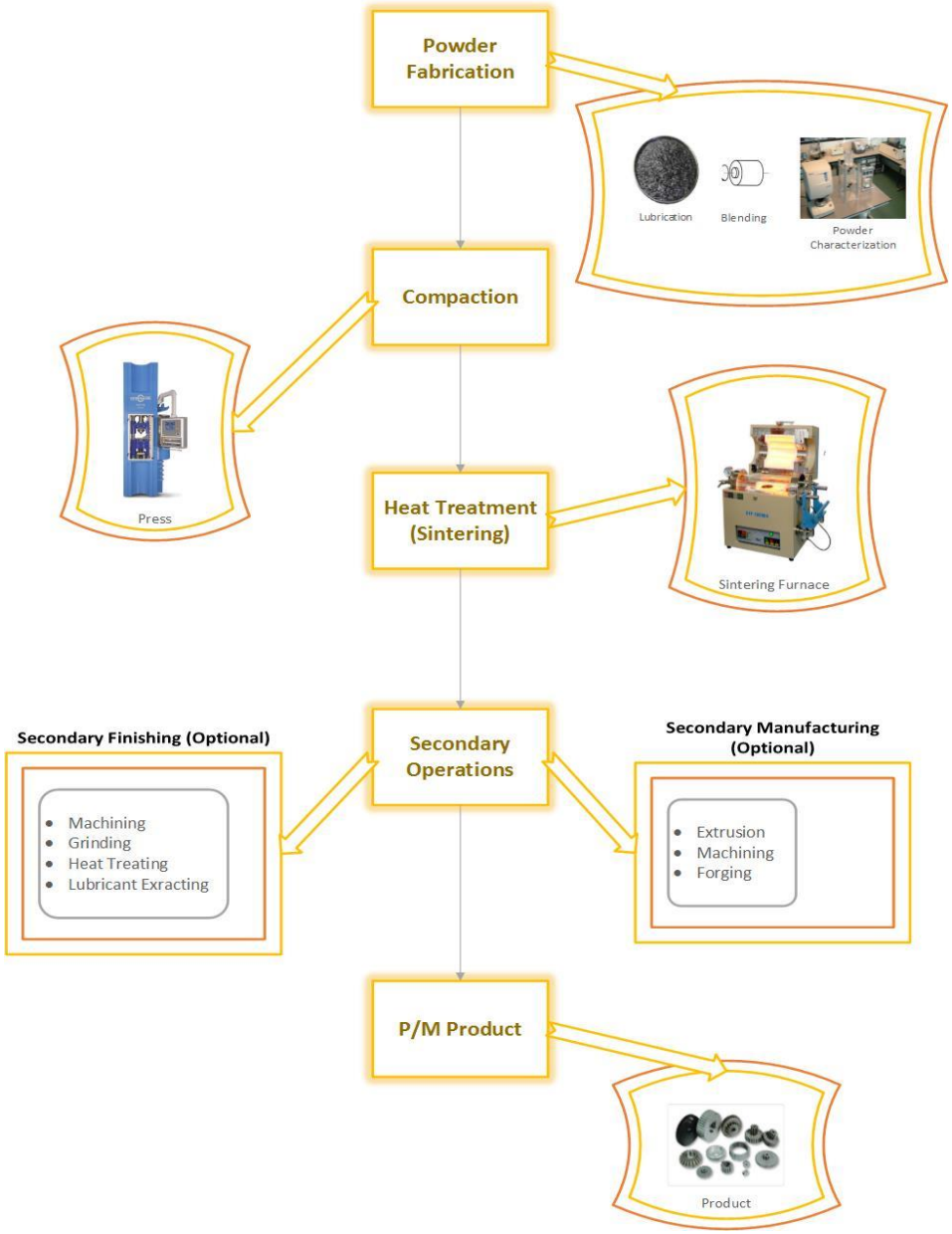

Figure 5. PM procedure with basic manufacturing steps (Chen et al., 2011).

1.3.1 Pressing

Compaction is the most important step in PM with respect to give final shape of the product by compacting under pressure to create weak van der Waals bonds between particles. Many parameters such as pressure, temperature, particle properties, internal friction (particle-particle), and external friction (particle-die and die-die) are effective

in compaction stage (Arifin et al., 2014; Bolzoni et al., 2013). Compaction process type is defined depending on the level of temperature and the direction of applied pressure. Compaction is divided into three subcategories according to existence of heating: cold, warm and hot compaction as in Figure 6. Compaction is also named based on the direction or axis of applied pressure such as die compaction and isostatic compaction.

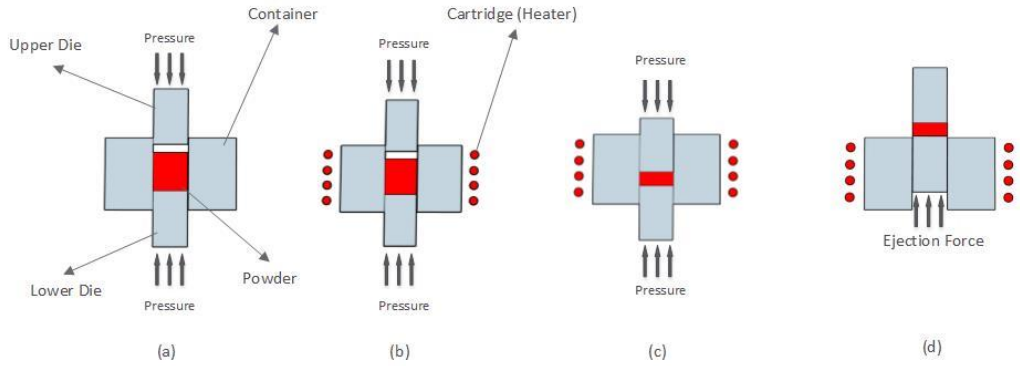

Figure 6. Representation of (a) cold and (b, c, d) hot/warm compaction.

The mechanism of compaction can be basically explained stage by stage. After the pressure starts to affect particles, they escape through the gaps and fill them. Particles are rearranged by themselves under the impact of the applied pressure. Simultaneously, elastic deformation occurs at the contact points. At the regions where the pressure exceeds the yield strength of material, plastic deformation occurs following by the permanent change in the shape of particles. Each mechanism does not occur separately but simultaneously. However, particle rearrangement only prevails at the lower pressure (Smith et al., 1998). Porosity or relative density is the most important output of a compaction process. The sufficiency of final product is highly dependent on relative density in terms of mechanical and physical properties.

There are many factors such as pressure (time, load and rate), temperature, particle properties (size, morphology, and homogeneity), lubrication, and material type of die and powder (friction coefficient, mechanical properties etc.) that can affect relative density and mechanical properties of the final product (Figure 7).

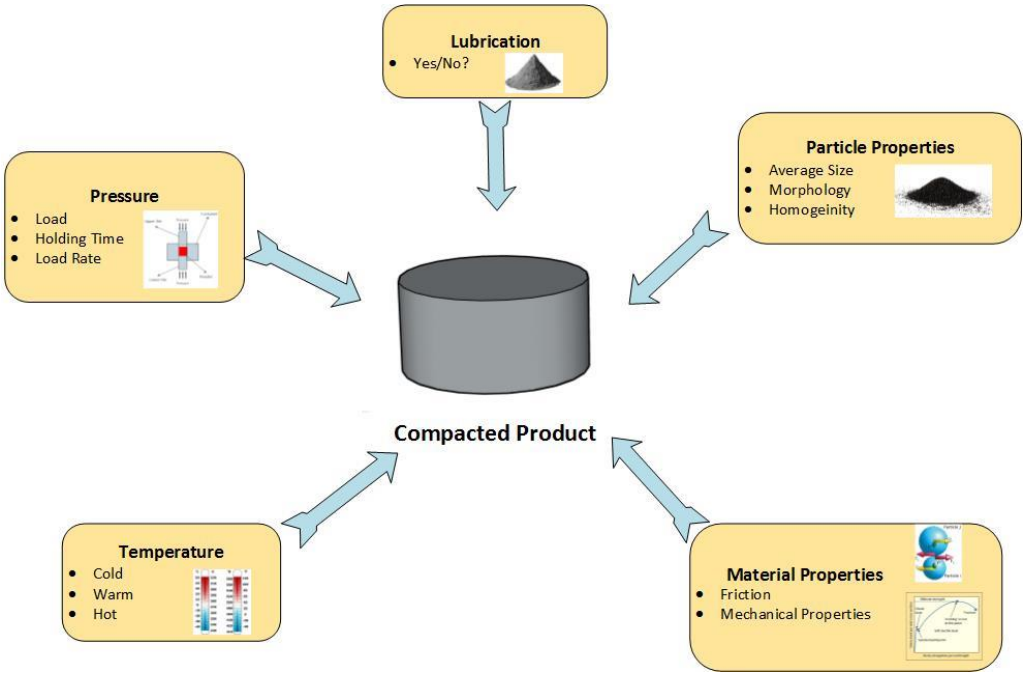

Figure 7. Dominant parameters on relative density in compaction.

Many studies on different metal powders proved that green density or relative density increases as applied pressure increases (Chen et al., 2011; Garg et al., 2007; Kang et al., 2007; Shukla et al., 2012). For instance, two types of molybdenum powders (Alldyne and Osram) were compacted under compaction pressure range of 280-840 MPa to understand densification behavior of molybdenum powders at room temperature (Garg et al., 2007). Average relative density of compacted specimens increases from 0.63 to 0.79 with the increase in compaction pressure form 280 to 840 MPa. It was also stated that coarser particles have better densification capability than finer ones as another significant result. The effect of compaction pressure has been studied under cold conditions on Ti alloy (Ti–6Al–4V) (Chen et al., 2011), Al alloy (Al 6061) and Fe powders (Kang et al., 2007). In these studies, wide spectrum of compaction pressures were applied to all powders such as Ti alloy (from 17 to 690 MPa), Al alloy (from 30 to 400 MPa) and Fe powders (from 100 to 800 MPa). The common feature of these studies was that compaction pressure has a significant influence on relative density. The effect of compaction pressure has been also studied in hot conditions. A Cu based material (Cu-Cr-Nb) was pressed under compaction

pressures of 10, 20 and 30 MPa at elevated temperatures (800, 900 and 1100˚C) (Shukla et al., 2012). The results showed that compaction pressure increased relative density in all compaction types (cold, warm, and hot).

Heating powder and lubrication are techniques mainly used for reducing required force to compact powders. These techniques are also used to manufacture high dense materials with PM technique. The effect of temperature during hot or warm compaction will be discussed later in hybrid method.

PM technique struggles with high friction forces (internal and external) since particles in micro scale have high specific surface area (the ratio surface area of a particle to its mass) (Simchi, 2003). Thus, lubrication was suggested by researchers as an enhancement to drawbacks in PM process such as inhomogeneity in density distribution due to internal friction, injection problems due to die-wall friction and excessive forces for compaction (Babakhani et al., 2006; Enneti et al., 2013; Nor et al., 2008). In order to prevent internal friction between particles, lubricants are applied in two ways: (1) they are mixed with powder and (2) applied to die wall. Mixing a lubricant with metal powders reduces internal friction between particles while applying lubricant to the tool surfaces reduces tool-particle and tool-tool friction (Nor et al., 2008). Consequently, both lubrication methods reduce slightly external and internal friction. This fact was proved in a study (Simchi, 2003) by comparing two application types of lubrication which are called as admixed and die wall lubrication. Cold compaction was conducted on alloys with 0.5%Mo and 3.0%Cr and lubricated with natural graphite UF4 iron powders under different pressure (150, 300, 450, 600, and 800 MPa) conditions. Admixed lubrication increased mechanical strength more than die wall lubrication by opening locks among particles at the pressure lower than 450 MPa. However, die wall lubrication increased the transmission of pressure into metal powders and played a big role in pore reduction in high pressure levels. Lubrication also made green bodies weaker at high pressures. As it has been previously stated, powder compaction process consists of several stages (rearrangement, elastic deformation, plastic deformation and fragmentation for brittle materials). At lower pressure, powder fragmentation is active so lubrication increases densification by reducing friction while lubrication

powders hinder plastic deformation and subsequently densification at higher pressure than elastic range (Simchi, 2003). Other lubricants such as ethylene-bis-stearamide (EBS), zinc stearate, and lithium stearate were applied (Babakhani et al., 2006; Enneti et al., 2013; Nor et al., 2008) to investigate the effect of lubrication on densification behavior of metal powders under different manufacturing conditions. Lubrications regulated metal powder flow by reducing internal and external friction and decreases non-homogeneous density distribution. It also increased the tool life by preventing wear. Similar to a previous study (Simchi, 2003), different amount of ethylene-bis-stearamide (EBS) (0.2-0.8 wt.%) and zinc stearate (0.25-2 wt.%) were used as lubricants in compaction of two iron alloy (ASC100.29. and AC1000) powders, respectively. ASC100.29 was compacted at a temperature of 130 °C while AC1000 was compacted at compaction pressure range of 276-689 MPa. As expected, lubrication aided to densification with reducing required force for compaction. Additionally, it smoothed the ejection of compacted parts. In both warm and cold compaction, the lubricated products were stronger than the unlubricated ones.

Particle size and size distribution and morphology are also critical parameters in compaction of metal powders. The effect of particle properties on compaction behaviors of metal powders was criticized below. For instance, spherical and spongy iron powders with average particle size of 15 μm were compacted at room temperature (Poquillon et al., 2002). Densification capability of spherical iron powders was higher than spongy powders because roughness on spongy powder surfaces was an obstacle for sliding particles on each other. Studies (Jabur, 2013; Rahimian et al., 2009) also showed that manipulating particle size has a direct impact on compressibility of metal powders. Increasing particle size reduced the density of bronze powders (Jabur, 2013). The same result was seen on the compaction of Al and Al_2O_3 mixtures. Density was increased with decreasing particle size of the composite. In cold compaction of iron-molybdenum powders (Chen et al., 2011), densification capability of that powder increased approximately 6% while particle size decreasing from 45 to 150 micrometers. The fact that higher particle size reduces densification was not changed in nanoscale (Saha et al., 2012). In compaction of alumina powders in 8 different size groups between (10-650 nm), the compacted powder group with the smallest particle size was the densest powder

group but the group with largest particle size was the most compressible group. In order to get better densification, it was suggested (Fedrizzi et al., 2012) to select particles from different size ranges. In addition to this, mixing soft and hard material will result in even better densification.

1.3.2 Post heat treatment (Sintering)

Sintering is a controlled-atmosphere heat treatment process that has a great influence on the properties of final product. Sintering consists of heating to below material melting point, remaining constant at that temperature and cooling again at room temperature (Bolzoni et al., 2013). Sintering triggers diffusion mechanism between particles that bond together during compaction (Smith et al., 1998). The difference between compaction and sintering is that sintering occurs by the effect of thermal energy without any external pressure (Boland et al., 2013). In sintering, pores are majorly eliminated by the time with the help of temperature (Figure 8).

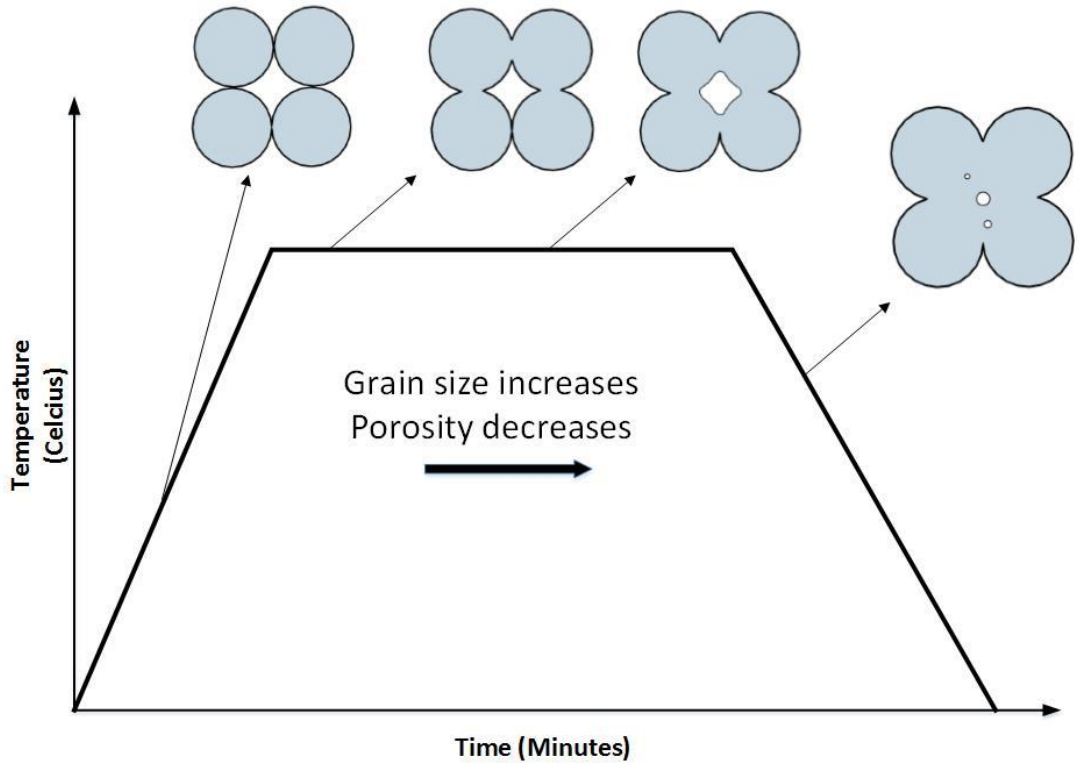

Figure 8. Decreasing porosity during heat treatment.

Dominant sintering parameters can be mainly listed: (1) sintering time, (2) sintering temperature, and (3) atmosphere (Dudek and Włodarczyk, 2013; Jabur, 2013; Kurgan and Varol, 2010; Xie et al., 2007). Many studies have shown that sintering parameters are very impactful on mechanical properties of sintered components. Boland et al. (Boland et al., 2013) found that there is an optimum sintering temperature and sintering time of 600^0C and 20 minutes for a novel Al–Cu–Mg alloy powder for the highest density. Jabur compared experimental and computational results and concluded that the bulk density of the sintered bronze powder increases as sintering temperature increases (Jabur, 2013). He also found experimentally that there is an optimum sintering time which result in the highest bulk density of a bronze powder. There are also studies on the effect of sintering atmosphere on porosity in literature (Dudek and Włodarczyk, 2013; Kurgan and Varol, 2010). Dudek and Włodarczyk used nitrogen and hydrogen atmospheres during sintering of compacted 316L stainless steel powders (Dudek and Włodarczyk, 2013). They observed that hydrogen atmosphere leads to higher porosity compared to nitrogen atmosphere. Kurgan and Varol also investigated the effect of sintering atmosphere on mechanical properties (Kurgan and Varol, 2010). They showed that specimens which are sintered under nitrogen atmosphere have superior mechanical properties than the sintered specimens under argon atmosphere.

Sintering can also be classified into two categories according to the level of sintering temperature levels of solid-state and liquid-state sintering. Xie et al. compared mechanical properties of magnesium alloy (Mg-9Al) which is sintered via solid state and liquid state sintering techniques (Xie et al., 2007). The liquid state sintered specimens have higher tensile and yield strength but lower ductility than the solid state sintered specimens. They claimed that brittle intermetallic phase ($Mg_{12}Al_{17}$) causes a reduction in the ductility of materials produced by liquid state sintering technique.

1.3.3 Hot Pressing

Hybrid method is another PM technique that both compaction and sintering are applied together. It is also named as hot or warm compaction. The purpose of this process is to get full density components and/or to reduce required forces for

densification. As the temperature increases, the yield strength decreases (Askeland et al., 2011). This relationship provides better densification under the same pressure (Askeland et al., 2011). Metal powders show better plasticity as the temperature increases and hence work hardening is by-passed (Dám et al., 2013).

1.3.4 Densification Fundamentals

Densification fundamentals during hot or warm compaction are based on three different mechanisms: (i) plastic deformation, (ii) power law creep and (iii) diffusional creep as shown in Figure 9 (German, 2005). Hot or warm compaction is conducted under different pressure and temperature conditions. This process is driven by both external and internal stresses. External stresses come from compaction pressure while internal stresses occur as a result of the increase in environment temperature (German, 2005).

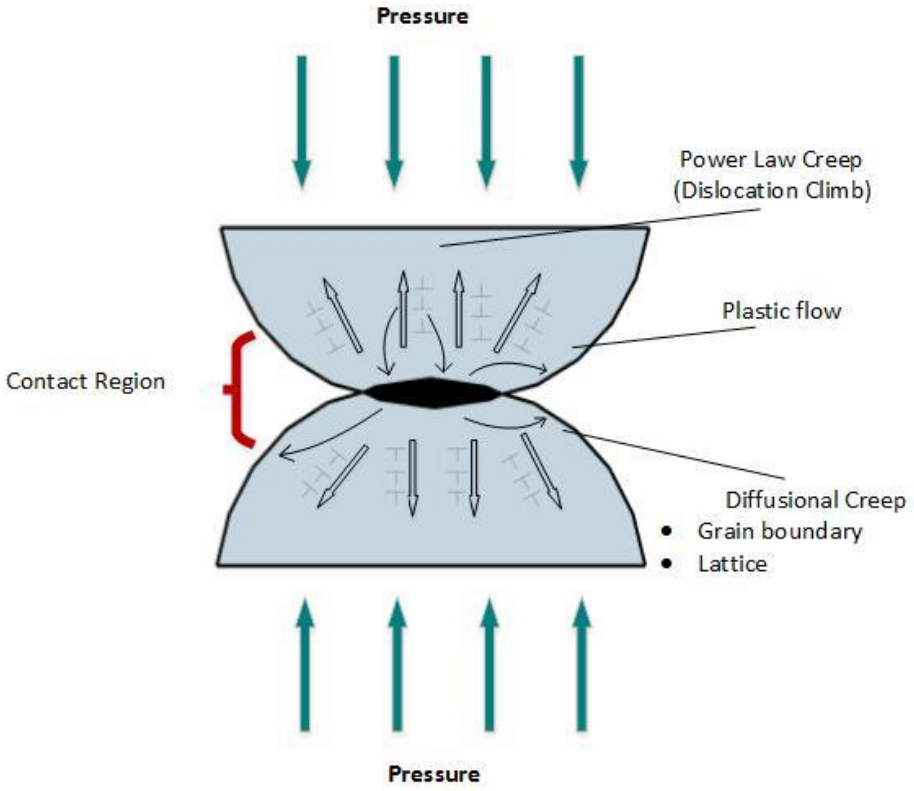

Figure 9. Densification mechanisms during hot/warm compaction (German, 2005).

German has explained densification mechanism during compaction at elevated temperatures (German, 2005). First mechanism is plastic deformation in which powder particles deform permanently at contact points where the normal stress exceeds the yield strength of material. Since most of materials become softer as a general material behavior, the yield strength is lower in hot/warm compaction than cold compaction. The impact of plastic deformation mechanism is limited by the condition which effective stress at contact points exceeds the yield strength of material. The other densification mechanism is power law creep which is especially influent when both stress and heat are applied. Dislocation climb occurs especially at high temperature by the movement of atoms in lattice structure even at low stresses (Jeong et al., 2012). Densification rate is highly dependent on the contact area between particles due to the increasing in the number of dislocation can climb. Third densification mechanism is diffusional creep that is the dominant mechanism in hot pressing and occurs by means of the movement of atoms due to the difference between compressive and tensile stresses. The direction of the movement of atoms is from high compressive stress to higher tensile stress during diffusional creep. There are two types of diffusional creep according to the type of formation. Diffusional creep can occur at grain boundaries (Nabarro-Herring creep) and lattice structures (Coble creep) (German, 2005). The three mechanisms are not sequential events and can take place simultaneously depending on environmental conditions such as temperature and pressure. Throughout densification, particles deform plastically and diffuse mutually by means of the mentioned mechanisms. As a result, pore elimination is achieved at the end of the process depending on fabrication conditions.

1.4 Aim of the Study

The aim of this study is to investigate the microstructural and mechanical properties of the Mg alloy discs compacted under pressures of 25 and 40 MPa and sintered for 30 and 150 min. The relative density was manually calculated and compared to computational and image processing results. X-ray diffraction (XRD), scanning electron microscopy (SEM), Brunauer-Emmett-Teller (BET) analysis were used to define the microstructural characteristics of the Mg alloy discs. The mechanical properties of the Mg alloy discs were investigated through diametral tensile and

Vickers microhardness tests. The effects of surface and manufacturing conditions on the biological properties were also studied by MTT cell viability test.

CHAPTER 2

MATERIALS AND METHODS

2.1 Material

AZ91 magnesium alloy powders having irregular shapes were used to manufacture surface modified porous specimens. Composition of powders, powder particle size and size distribution and particle shapes were characterized before experimental procedure. The particle size distribution and shape were also characterized through a particle sizer machine (Malvern Mastersizer 3000, UK) and Quanta scanning electron microscope (FEI Inc., USA), respectively. General composition of AZ91D metal powders is represented in Table 4 (ASTM Standard B 93/B 93M).

Table 4. Nominal chemical composition of AZ91D magnesium alloy in weight percentage.

Mg	Al	Zn	Mn	Ni	Cu	Si	Fe	Be	Other elements each
Balance	8.5-9.5	0.45-0.9	0.l7-0.4	0.00l	0.025	0.05	0.004	0.0005-0.0015	0.01

2.2 Experimental design

The sample discs were manufactured through powder processing under experimental conditions according to Table 5. Compaction pressure, sintering time and surface condition were employed as variables during the experimentation. Compaction pressure and sintering time have been defined as effective variables during feasibility experiments. The aim was to manufacture highly porous Mg alloy discs. Thus, compaction pressures were selected as 25 and 40 MPa. Higher than these compaction pressures (25 and 40 MPa) led to the discs with limited porosity. Sintering times were also selected as 30 and 150 min. Longer sintering times did not affect physical

properties of the discs. Furthermore, it caused the formation of secondary phases in the discs. Surface condition was changed to evaluate the effect of surface structures on the biological properties as well as mechanical integrity. During the all experimentation, sintering and compaction temperatures were fixed to 380 and 150^0C, respectively. In preliminary experiments, these sintering and compaction temperatures showed best mechanical and physical performance. Thus, these parameters were not considered as experimental variables.

Table 5. Experimental conditions

Experimental parameters	Level I	Level II
Compaction pressure	25 MPa	40 MPa
Sintering time	30 min	150 min
Surface condition	Smooth	Textured
Constants: Sintering temperature: 380°C and Compaction temperature: 150°C		

A 2-level full factorial experimental design with three parameters was used (Table 6). The Mg alloy disc samples are notated by numbers. In the next chapters, these notations are be used in graphics and images.

Table 6 Two-level full factorial experimental design.

Notation	Compaction pressure (MPa)	Surface Condition	Sintering Time (min)
1	40	Smooth (1)	30
2	40	Smooth (1)	150
3	40	Textured (2)	30
4	40	Textured (2)	150
5	25	Smooth (1)	30
6	25	Smooth (1)	150
7	25	Textured (2)	30
8	25	Textured (2)	150

The diameter of the discs was defined as 20 mm. The discs with smooth and textured surface are represented in Figure 10. The textured surface had an approximate aspect ratio of 1.25. The width and height of the channels were 200 and 160 μm, respectively. The dimensions were selected in the light of the possible biological behavior of the seeded cells.

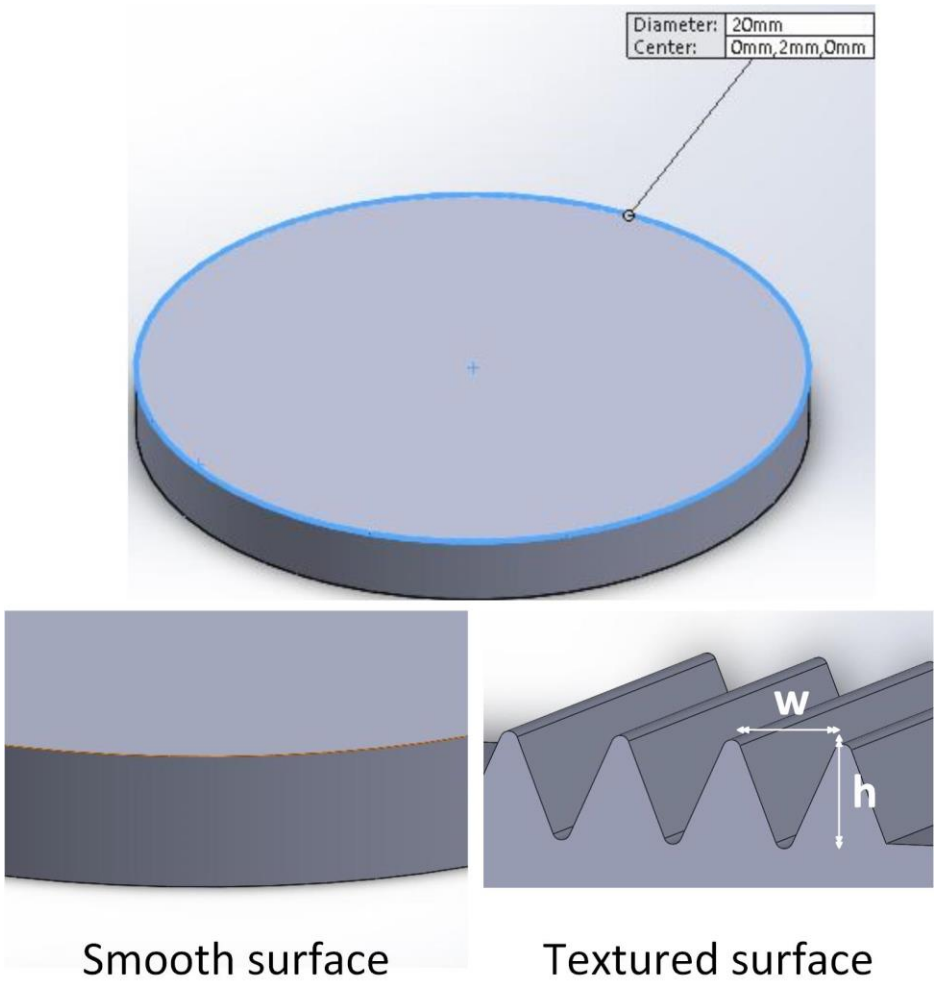

Figure 10. 3D representation of the Mg alloy discs with smooth and textured surfaces.

2.3 Sample manufacturing

The Mg alloy discs were prepared through PM process. As it has been stated before, there are two main stages that affect the material properties of PM products: (1) compaction and (2) heat treatment (sintering).

2.3.1 Compaction stage

During compaction experiments, an experimental setup consisting of (1) press machine, (2) press control unit, (3) hydraulic pumping unit, (4) temperature control

unit and (5) die system was used to manufacture surface-modified porous green bodies (Figure 11).

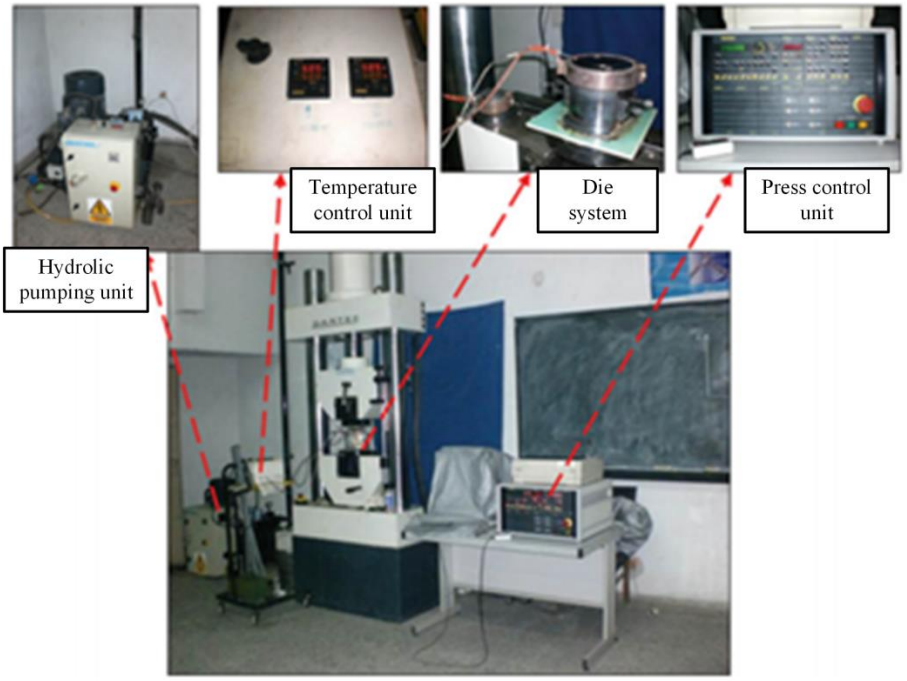

Figure 11. Experimental setup in compaction stage.

The powders were pressed by using Dartec Universal Testing Machine. The machine was active in both direction (up and down) but only compression direction was used to press. The loading capacity of the machine for compression was 600 kN. Press control unit enabled to control the movement of the press. The loading profile was identified into the control unit. Forces were applied as 7.85 kN and 12.56 kN which corresponded to 25 MPa and 40 MPa. Standardization in the loading force was ensured by the control unit in every experiment. A hydraulic pump was used to provoke the press for compacting. A surface-modified die was used to form the powders. The die system was made from H13 tool steel. H13 tool steel was selected as die material because it has enough strength for compression and is durable even at elevated temperatures. The powder poured into the die cavity and leveled with an object with smooth surface. The height of poured powders was measured by adjustable part of die system. After upper part of the die system was mounted on the powders, compaction was conducted. The die system was heated by the temperature

control unit. The temperature was controlled by using K-type thermocouple (Tetcis Ltd. Şti., Ankara, Turkey) during compaction. The temperature control unit allowed regulating working temperature up to 400^0C which is higher than the temperature used in the experiments.

2.3.2 Heat treatment (sintering) stage

Heat treatment process was conducted in a quartz-tube furnace (OTF-1200X, MTI Corp., CA, USA) as seen in Figure 12. The furnace has a maximum sintering temperature of 1200 °C. The temperature increase rate is 10°C/min. An inert gas ($95\%N_2+5\%H_2$) was pumped into the furnace during the experiments to prevent oxidation. Compacted Mg alloy discs sintered for 30 and 150 min at a sintering temperature of 380°C. Temperature profile was set by the control panel. Temperature was measured by thermocouples and kept stable during all experimentation.

Figure 12. Sintering furnace with quartz tube and control panel.

In this study, Mg-Al binary phase diagram was used to define applicable sintering temperature range. A solid state sintering was conducted to benefit from mechanical interlocking effect. In the light of the binary phase diagram, applicable sintering temperature range was selected between 330 and 520°C, which is the corresponding point to the magnesium composition as seen in Figure 13 (Dahle et al., 2001), which

is distinguished with red lines. At last, it was decided that sintering temperature of 380°C would be a good choice to benefit mechanical interlocking among metal powder particles.

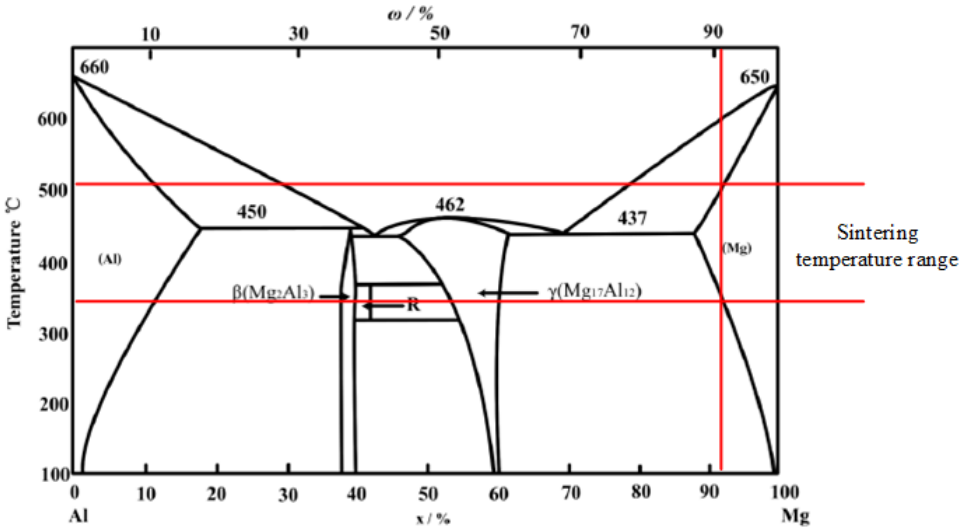

Figure 13. Mg-Al binary phase diagram (Mastai, 2013).

2.4 Physical analysis

2.4.1 X-ray diffraction analysis

The phases of the Mg alloy discs sintered for various time and as-received powder were characterized by XRD method. For XRD analyses, Rigaku Ultima-IV X-beam diffraction device (Japan) was used. The specimens were exposed to Cu-Kα radiation and scanned from different angles between 20º and 80º with the scan rate of 2.0º/minute. The results were compared with Joint Committee on Powder Diffraction Standards JCPDS files.

2.4.2 Scanning electron microscopy

During experimentation period, as-received, the compacted and heat-treated metal powders were observed from different perspectives by scanning electron microscopy (SEM). QUANTA 400F Field Emission (FEI Inc., USA) with high resolution of 1.2 nm was used to take SEM images. These images were then used for microstructural evaluation.

2.4.3 Relative density

Relative densities of the Mg alloy discs were calculated manually. The fundamental equation of density, equal to mass per volume, was used to calculate the apparent density of the discs. Apparent density was divided by the theoretical density of AZ91D magnesium alloy to find a relative density value. Density of bulk AZ91D magnesium alloy was taken as 1.82 g/cm^3 (Zhang et al., 2015).

Image processing technique is a simple, fast and reliable method for porosity measurements. This technique was used to compare porosity values to manually-calculated relative density values. Microscope of cross-section views of samples converted into black and white format from gray scale by using ImageJ software (National Institutes of Health, Bethesda, MD, USA). The same technique was used to convert images. At least three images were captured from each cross-sectional views.

2.4.4 Brunauer-Emmett-Teller (BET) Surface Area Analysis

Surface area analysis of as-received and the Mg alloy discs was conducted through Autosorb-6 surface characterization device (Quantachrome Corp., US). The analysis lasted approximately one hour for each specimen under nitrogen gas atmosphere at 150°C. At least 7 measurements were taken from the surface of each sample. A specific surface area was measured from the surface of each specimen.

2.5 Mechanical tests

2.5.1 Diametral tensile test

Diametral tensile test (DTT) is a simple method to indirectly evaluate tensile strength of low strength or brittle materials (Huang et al., 2012a). It has been used to investigate the mechanical properties of ceramics, pharmaceutical disks, rock materials etc. (Jonsén et al., 2007). It has been also reported that it is an applicable method for powder processed materials (Jonsén et al., 2007). In this technique, a complex geometrical shape is not required as in tensile test but simple circular disk is sufficient to conduct the test (Huang et al., 2012b). Diametral tensile strength has also direct correlation with elastic modulus, compressive strength, hardness and

fatigue as reported (Della Bona et al., 2008). However, the one problem with DTT is that a huge amount of energy storage before fracture causes some fluctuations in the results (Swab et al., 2011). Diametral tensile strength was calculated from Eq. 5.

$$\text{Diametral tensile strength} = 2F/\pi DT \quad (5)$$

where F is the load at fracture, D is the diameter and T is the thickness of the disk.

Material behavior can be predicted from the type of crack after the test. If the specimen is broken into two parts then it refers to a homogenous stress distribution (Zaytsev and Panfilov, 2014). Numerous cracks (more than 4) are attributed to high elastic energy storage in the disk (Souto et al., 2011; Zaytsev and Panfilov, 2014). Beyond that, long cracks with blunted tips are due to high plasticity while short cracking with a sharp tip is the result of high elasticity (Zaytsev and Panfilov, 2014).

In this study, the Mg alloy discs were broken in diametral tensile test to evaluate fracture behavior and indirect tensile strength. A LS 500 model test machine (Lloyd Instruments) was used to apply axial load on the Mg alloy discs. Each test replicated three times (n=3) to ensure statistical reliability. A stress-strain curve for each test was obtained from the collected data through a computer controlled data acquisition system.

2.5.2 Vickers hardness test

Vickers micro-hardness measurements (Type II) were performed by a HMV-2 Vickers micro hardness tester (Shimadzu Co., Kyoto, Japan). Samples were, first polished with SiC papers (Buehler Ltd., Lake Bluff, IL, USA) from 200 to 1200 grades and then they were polished with a 1µm monocrystalline diamond suspension (Buehler Ltd., Lake Bluff, IL, USA). At least 10 measurements were performed on each sample with a diamond indenter at 19.61 N load for 20 seconds. The average Vickers hardness was calculated using the formula below:

$$HV=0.001854(P/d^2) \quad (6)$$

HV: Vickers hardness; P: Applied force (N); d: Average length of two diagonals (mm).

2.6 Computational analysis

Density distribution is main problem in powder processed products due to particle-particle and wall-particle friction. Morphology and mechanical properties of particles are also important for density distribution. Inhomogeneous density distribution affects mechanical properties of the product and hence it causes distortions during heat treatment process. Numerical analysis allows predicting inhomogeneous density or stressing distribution that enables to get high quality products (Khoei et al., 2012; Pizette et al., 2010).

Numerical analysis is a well-known method to evaluate mechanical and physical properties in PM (Jeong et al., 2015). Numerical analysis has been conducted in two ways as discrete and continuum models. In discrete model, particular metal powder particles are analyzed one-by-one while continuum model is used to evaluate bulk materials. In this study, computer aided solid modeling and numerical simulations are conducted to predict density distribution of the Mg alloy discs. For the sake of completing analysis in shorter time, continuum model was used. A computer equipped with Intel Core i7 2.20 GHz processor and 8 GB RAM was used. As software, Abaqus (Dassault Systemes Corp., France) was used.

To run a simulation, material data of the Mg alloy discs should be known. Some of the data was collected form the literature. However, others were obtained through an experiment. Particle-particle friction was found in shear friction test. Shear friction test was conducted by using U-test test machine (220-240V and 50-60 Hz). Three levels of normal stress were applied to the die surface (100mm*100mm). Shear velocity was constant to 1.0 mm/min. The friction coefficient in terms of Mohr–Coulomb friction theory was calculated as following equation.

$$Ί = \sigma \tan(\phi) + c \qquad (7)$$

where Ί refers shear strength, σ, normal stress, ϕ, internal friction angle and c, cohesion in the equation. According to the Mohr-Coulomb model in Figure 14, angle of internal friction (Φ) and the cohesion (c) were found as 30.37° and 81.33,

respectively. The model has given an internal friction coefficient of 0.53, which was then implemented into the software for computational analysis.

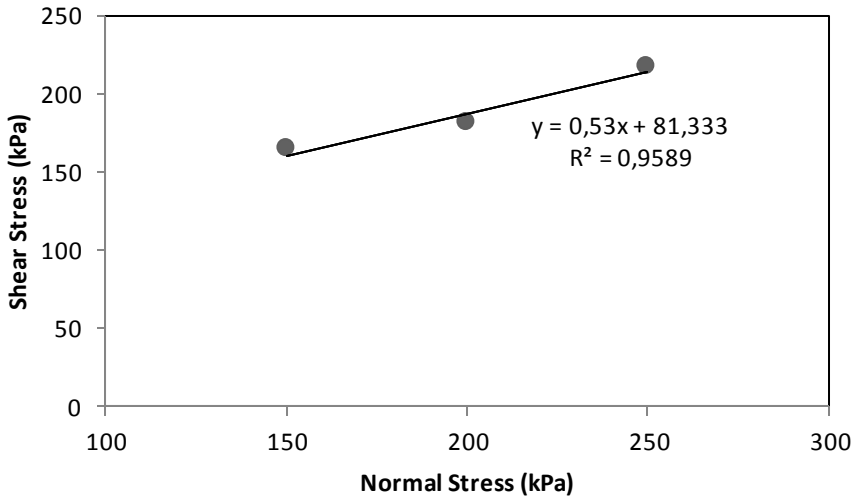

Figure 14. Mohr-Coulomb model of Mg alloy powders for the friction coefficient.

As stated before, physical and mechanical material parameters should be obtained in order to conduct numerical analysis. Necessary parameters have been gained either from shear test or the literature (Table 6). In the analysis, von Mises material model was used. Strength coefficient (K) and strain-hardening coefficient (n) were defined as following equation where ε is strain and σ is stress.

$$\sigma = K\varepsilon^{n} \tag{8}$$

The relative density of the Mg alloy as loose powder was calculated by precision scales. The volume and weight of the uncompact powder were used to calculate the density of the loose powder. The calculated density was then divided by the density of bulk AZ91D Mg alloy.

Table 7 The material parameters of AZ91D Mg alloy.

Material property	Symbol	Unit	Value	Reference
Relative density as loose powder	Φ	%	0.42	Calculated by precision scales
Strain-hardening exponent coefficient at 150ºC	n	-	0.06	(Yoshihara et al., 2005)
Strength coefficient at 150ºC	K	MPa	290	(Yoshihara et al., 2005)
Poisson's ratio	ν	-	0.33	(Sumitomo et al., 2002)
Elastic modulus as a function of relative density	E	GPa	43.02-49.05	(Sumitomo et al., 2002)
Die-die and die-wall friction coefficient	f_1	-	0.08	Software default
Particle-particle friction coefficient	f_2	-	0.53	Found in shear test.

2.7 Cell viability

Methylthiazolyldiphenyl-tetrazolium (MTT) assay was conducted to measure hFOB (human fetal osteoblastic) cell viability on the surface of the Mg alloy discs prepared via PM route. Before cell viability examination, all Mg alloy discs have been exposed to gamma radiation (25 kGy) for the sake of decontamination. Sterilization was conducted in Turkish Atomic Energy Authority (TAEA) facilities. In order to get the cell growth process, a mixture containing DMEM/HAM's F12 (GibcoLife Technologies, UK), 15% FBS (Merck Millipore, Germany) and 0.1% penicillin (Merck Millipore, Germany) was used. The cells were then incubated in a humid

environment containing 5% CO_2 at 36.5^{0}C until the cells reached to confluence. After the completion of cell growth process, the cells were seeded on the surface of the discs (30,000 cell/cm^2) and then the seeded discs were incubated for 3 and 7 days in the incubator (5215, Shel Lab., USA). The medium of the seeded cells was renewed every 2 days. The MTT assay proceeded at the end of each time period.

The cytotoxicity of the Mg alloy discs was analyzed through MTT assay. MTT solution (AppliChem GmbH, Germany) was added to each well where the discs were placed and then the discs were kept for 4 hours in dark due to high light sensitivity of the MTT solution. Apart from discs subjected to MTT test, an empty well was seeded and measured in each run in order to obtain positive controls. MTT solution was reacted with viable cells that induced colored formazan. Phosphate buffer saline (PBS) was used to solve insoluble formazan crystals by dimethyl sulfoxide (DMSO). A microplate reader (BioTech Instruments Inc., USA) was used to define the absorbance of the solution at 570 nm with a reference wavelength of 655 nm.

2.8 Statistical analysis

ANOVA test was conducted in order to distinguish statistical difference in the cell viability results. In one-way ANOVA test, Tukey's multiple comparison test method was used as post-hoc evaluation. The statistical test was run in SPSS 18 software. Statistical difference was regarded significant in case $p \leq 0.05$.

CHAPTER 3

RESULTS AND DISCUSSION

3.1 Physical analysis

3.1.1 Powder characterization

The average particle size was measured approximately as 100 μm with laser diffraction method. At the same time, the powders exhibited a wide variation in their size of 10% < 50.4 μm, 50% < 177.6 μm and 90% <614.1μm. Furthermore, the morphology of the Mg alloy powder particles was irregular and some of them had needle-like shape.

3.1.2 XRD analysis

XRD patterns of as-received powders and the sintered discs for 30 and 150 min are presented in Figure 15. Mg (JCPDS file no: 04-0770), Al (JCPDS file no: 01-089-4037), $Mg_{12}Al_{17}$ (JCPDS file no: 1-1128), and Al_2O_3 (JCPDS file no: 46-1212) were detected in XRD analysis. All samples mainly consist of Mg phase. All peaks became more intense and/or sharp in the discs sintered for 30 and 150 min when compared to the Mg peaks of as-received Mg alloy powder. It can be concluded that sintering process caused more crystallinity in the microstructure. It can also be deduced that the amount of Mg phase increased in the sintered discs at 380ºC compared to the as-received powder. However, as sintering time increased from 30 to 150 min, the Mg peaks intensity and sharpness decreased. Moreover, the peaks were shifted to the left for longer sintering time, which refers a distortion in the crystal structure.

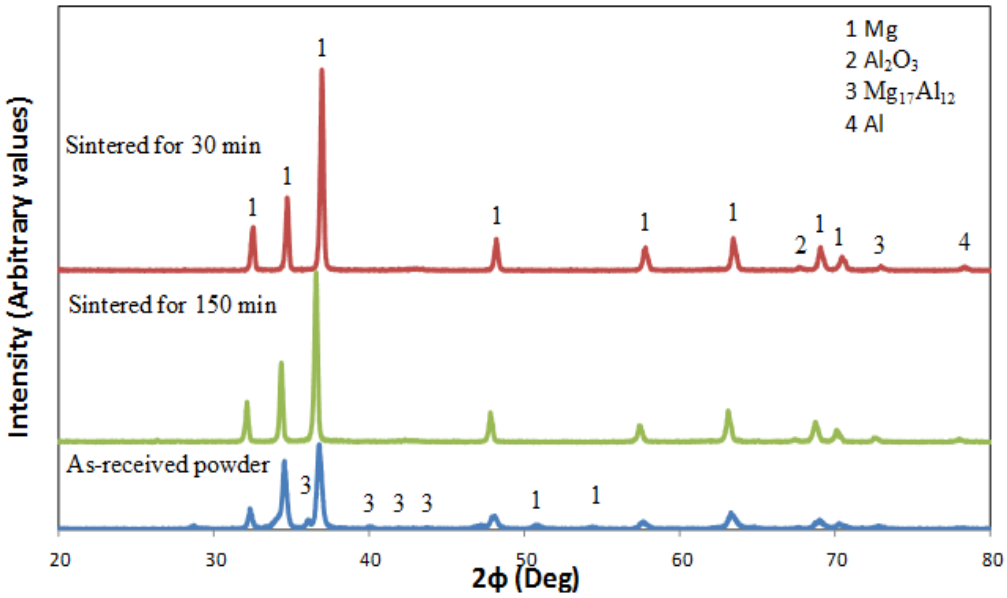

Figure 15. XRD patterns of as-received powder and the Mg alloy discs sintered for 30 and 150 min.

3.1.3 SEM observation

The existence and dimension of pores on the surface were investigated by SEM images. The SEM images of the Mg alloy discs are presented in Figure 16. Figure 16.a, b, c, and d shows the SEM images of the Mg alloy discs with textured surfaces. The pores greater than 100 µm were detected on the surface of the discs, which is necessary for cell activity. Moreover, it was observed that the dimension of pores varied from 10 to 100 µm. A specific pore size on the surface of an implant is required due to the dimensional concerns (Fu and Soboyejo, 2009; Mirhosseini et al., 2007). Otherwise, it is not possible that a cell cannot pass through small pores. In a study, it was claimed that the surface with pores in dimension of 10-120 µm increased cell attachment and proliferation (Fu and Soboyejo, 2009). Beneficial side of porous surfaces in this pore size range does not only increase the cell attachment and proliferation but also helps to improve the corrosion resistance of implants (Wu et al., 2013).

The formability of the surface structures was also investigated by measuring the surface structures. The width of the periodic surface structures was designed as 200

μm for the sake of easy attachment of cells on the surface. The height was also intended to manufacture as 160 μm. The average width of the surface structures for each surface was measured on the SEM images. It was measured for samples #3, #4, #7 and #8 as 209.1, 197.6, 206.4 and 205.4 μm, respectively. According to these results, the surface structures were formed successfully by the manufacturing process. The height was also measured. It was intended to manufacture the height with a value of 160 μm while the measured value was 164 μm. The aspect ratio was also intended to manufacture as 1.25. However, they were formed as 1.27, 1.20, 1.26 and 1.25 for the Mg alloy discs notated as 3, 4, 7 and 8, respectively. The height of the surface structures was also measured as 164.3 μm but the picture was not given.

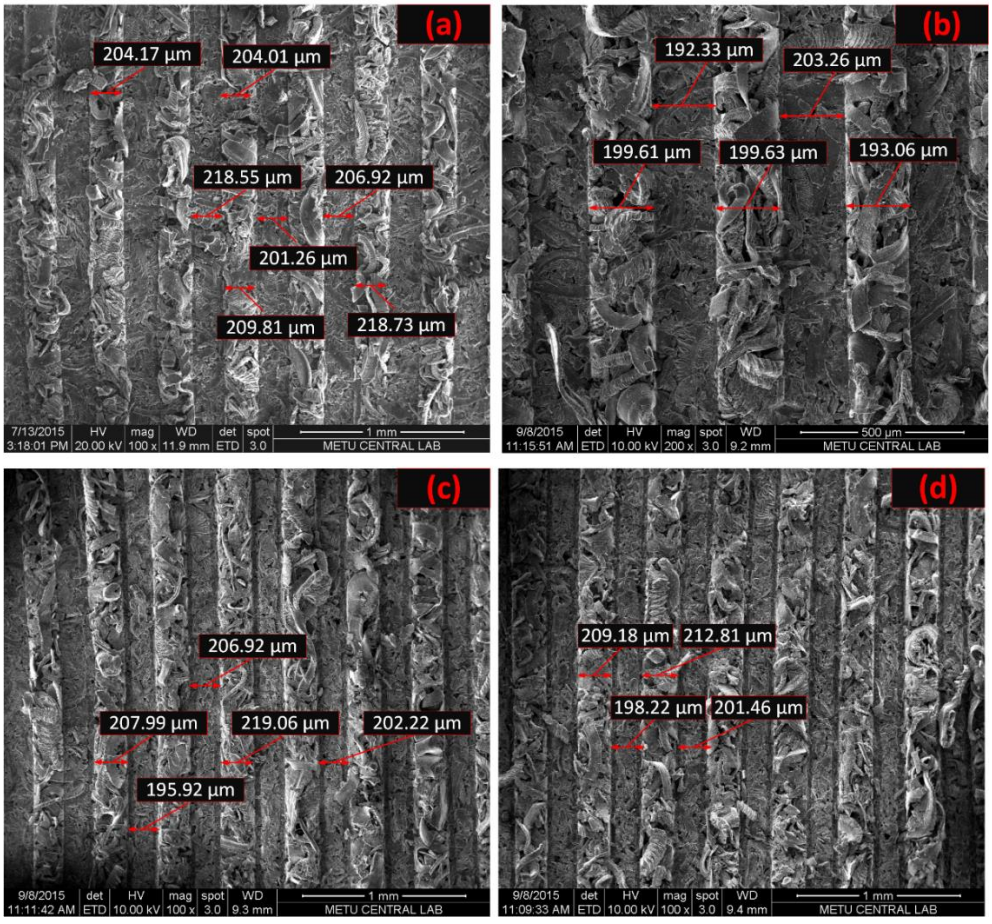

Figure 16. SEM images of the Mg alloy discs: (a) sample 3, (b) sample 4, (c) sample 7 and (d) sample 8.

The formation of pores on the surface of an Mg alloy disc (#1) was evaluated through three SEM images with various magnifications (Figure 17). Pore formation was observed on the surface which is a necessity for cell penetration and growth. In Figure 17.a and b, greater pores were observed while smaller pores were visible in Figure 17.c.

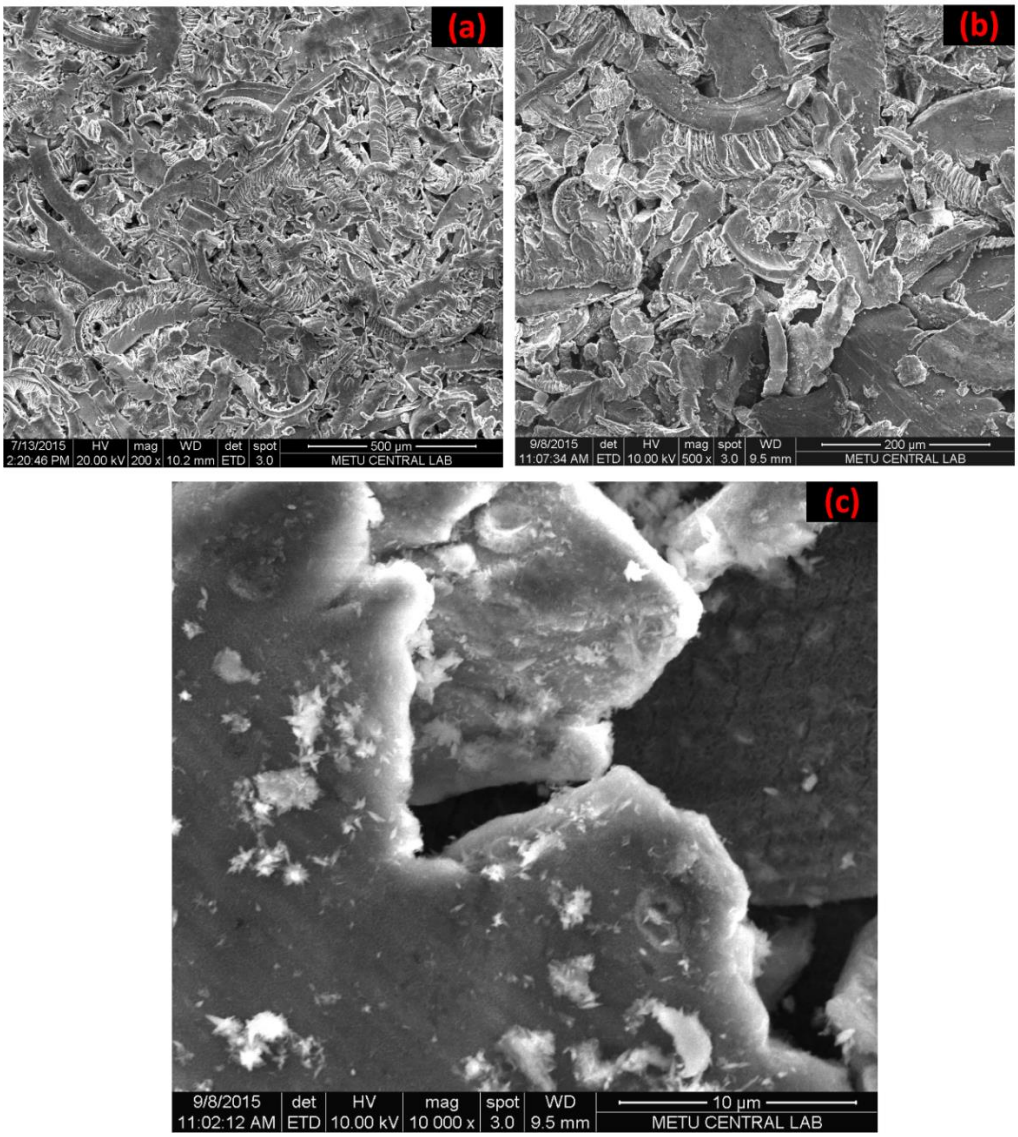

Figure 17. SEM images of the disc with a smooth textured surfaces with various magnifications of (a) 200x, (b) 500x and (c) 10,000x.

3.1.4 Relative density

Relative density is vital in biomedical materials with porous structure in terms of both mechanical and biological response. In literature, many attempts have been made to produce Mg-based scaffolds (Aghion and Perez, 2014; Li and Zheng, 2013; Staiger et al., 2010; Wen et al., 2001; Wen et al., 2004; Witte et al., 2007; Xia et al., 2013). The porosity of porous Mg alloy discs has ranged from 35 to 78% and their pore size distribution are between 10 and 1000 μm. Although porosity and pore size distribution are vital for biological activities such as cell adhesion and proliferation, highly porous structures decrease the mechanical properties (Witte et al., 2007). In this study, the relative densities of the Mg alloy discs were between 57 and 68%. In another word, the porosities varied from 33 to 43% as seen in Figure 18. It can be concluded that the obtained porosity values are acceptable from both biological and mechanical point of view.

Many parameters (compaction and sintering variables) are effective in material properties of processed powders. In this study, the relative densities of the Mg alloy discs increased as the compaction pressure increased from 25 MPa to 40 MPa according to Figure 18. It is a well-known fact that compaction pressure eliminates pores and decreases porosity in powder processed materials (Jabur, 2013). In PM process, it was proved that compaction pressure decreased relative density regardless of the type of material as in this study. The relative density of two molybdenum powders decreased as compaction pressure increased in the range of 280-840 MPa (Garg et al., 2007). The same effect was valid for other metallic powders which were compacted in a wide range of pressure spectrum (Chen et al., 2011; Kang et al., 2007). This effect was also dominant where low compaction pressures (10-30 MPa) were used (Shukla et al., 2012). In this study, a compaction range of 25-40 MPa was used and the same effect was observed on the relative densities. Thus, the result was compatible with the investigations in the literature.

On the other hand, sintering time (30 and 150 min) did not cause any significant change in relative densities. There is a general tendency that sintering parameters (including sintering time) have optimum values for the best relative density (Kurgan, 2014). However, similar to this study, specific sintering time varying from powder to

powder did not change relative density of the metal powders. The relative density of compacted bronze particles did not change at sintering times of 45 and 60 min (Jabur, 2013). Thus, sintering of the Mg alloy discs for 30 and 150 min may not be an effective way to reduce the porosity. It can be interpreted that a distinct change in the relative density might be obtained with longer sintering times.

The effect of surface condition was also investigated as smooth and textured surfaces which were designated as 1 and 2, respectively. Regardless of compaction pressure and sintering time, the relative densities decreased when surface was not smooth. There are not many studies that investigate the effect of surface condition on the relative density. Nonetheless, it can be commented that open pores on the surface may compensate further shrinkage of the Mg alloy discs. Moreover, the Mg alloy discs with smooth surfaces are expected to shrink more due to high energy storage capability than the discs with pores. The textured surface was able to cool more quickly which prevents further shrinkage.

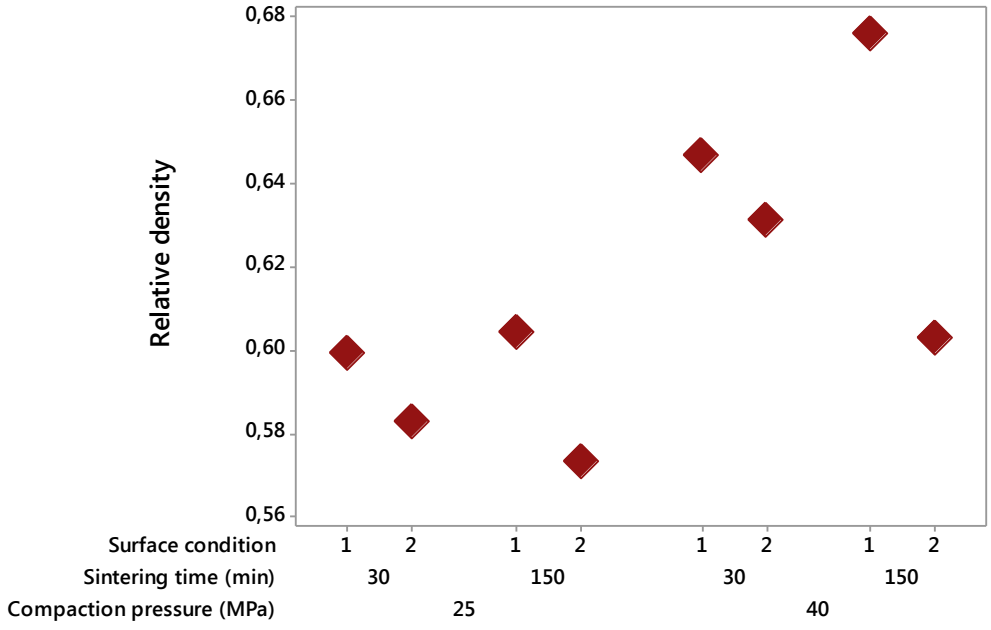

Figure 18. The effect of manufacturing conditions on the relative densities of the Mg alloy discs.

Additional experiments were conducted to investigate the sintering effect. The sintered and unsintered Mg alloy discs were compared to understand the effect of heat treatment on the relative densities. All of the Mg alloy discs were compacted at 25 MPa to remove the effect of compaction pressure on the relative densities. The sintered Mg alloy discs were heat-treated at 380^0C. In Figure 19, it can be seen that the sintered Mg alloy discs had higher relative density than that of the unsintered discs. The average relative density of the sintered Mg alloy discs was 0.56 while the sintered discs had an average relative density of 0.60. As it is known, sintering parameters (heating rate, sintering time, temperature and atmosphere) have a great influence on the relative density of the compacted powders (Yang et al., 2015). Optimum sintering conditions can maximize the material properties including relative density. Owing to Hall-Petch relation, exposing the compacted powders to heat for a specific time causes grain growth and decreases density (Hussein et al., 2015). In this investigation, sintering caused an increase in the relative densities of the discs. Results proved that heat treatment process caused grain growth by the effect of temperature which caused further densification (Kurgan, 2014).

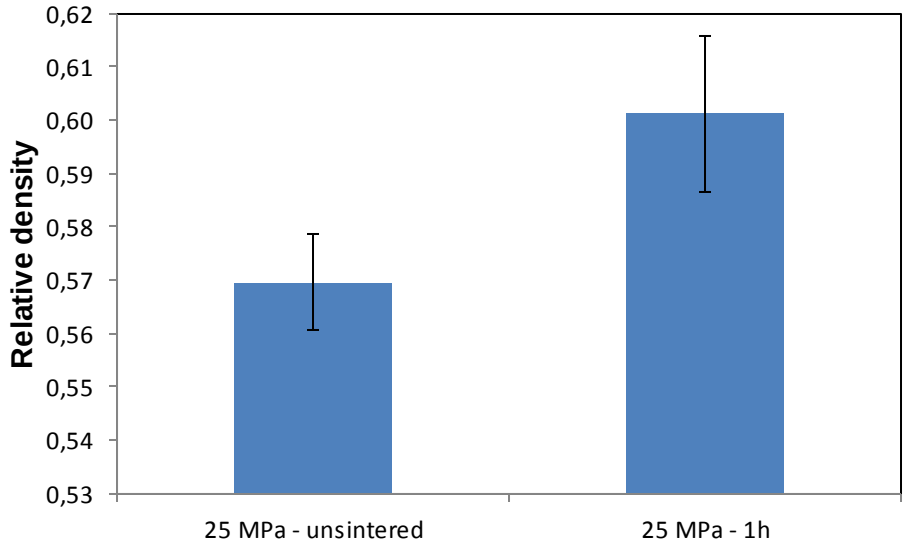

Figure 19. A comparison on the relative densities of sintered and unsintered Mg alloy discs.

Image processing results were compared to manually-calculated relative density values in order to verify the reliability of image processing method. Most of the

results were matched with manually-calculated relative density values (Figure 20). The reason of these mismatches can be related to irregular shape of particles and grinding process for metallographic observation. However, image processing technique was successfully implemented in this study. If metallographic observation processes (rough grinding, fine grinding and polishing) were conducted carefully and successfully, the better results would be obtained. It seemed that the metallographic preparation was highly successful for the Mg alloy discs notated as 1 and 2. The constant error was observed for samples between 4 and 8, which was acceptable because this error can be estimated. Beyond that, many attempts were made on the image processing technique and these studies were accomplished to implement (Liu et al., 2011; Mazzoli and Favoni, 2012).

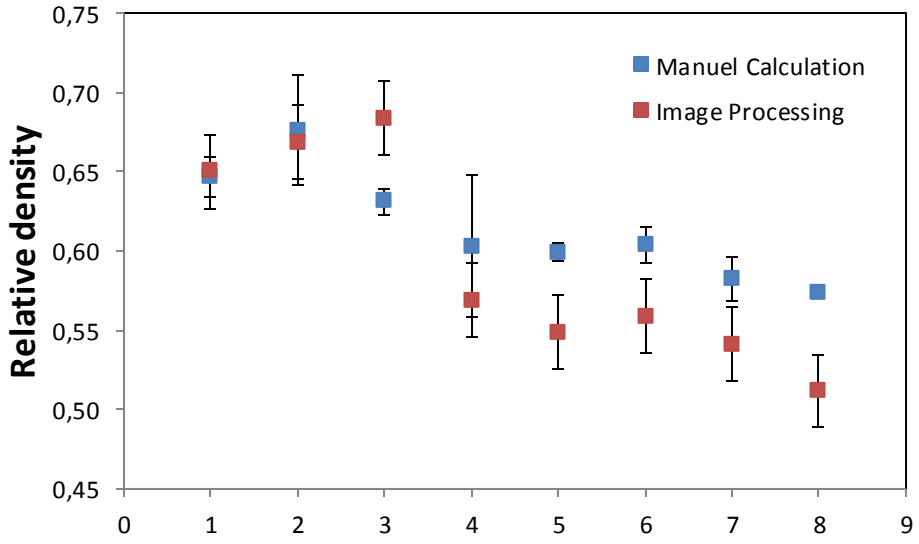

Figure 20. A comparison of relative densities between manual and image processing calculations.

The light microscopy (a, c, e and g) and image processed pictures (b, d, f and h) are represented in Figure 21. It was clearly observed that particles were completely bonded to each other after the sintering. The morphological properties and bonding quality were evaluated using light microscopy besides SEM. The light microscopy images proved that porous structures can be manufactured using powder compaction method. The validity of image processing technique was evaluated through the images. The transition from the light microscopy images to black/white ones was

successful as seen in Figure 21. The other conclusion is that compaction direction was observed from the deformation of particles. The Mg alloy particles were squeezed at the direction of the compaction. Greater than 100 μm pores were also observed in the structure of the discs which is required for cell ingrowth and proliferation (Brånemark et al., 2011; Fu and Soboyejo, 2009; Mirhosseini et al., 2007). They claimed that pores around 100 μm on the surface as well in the structure increased osseointegration at the bone-implant interface. Thus, pore size and distribution were convenient in this study according to the mentioned studies.

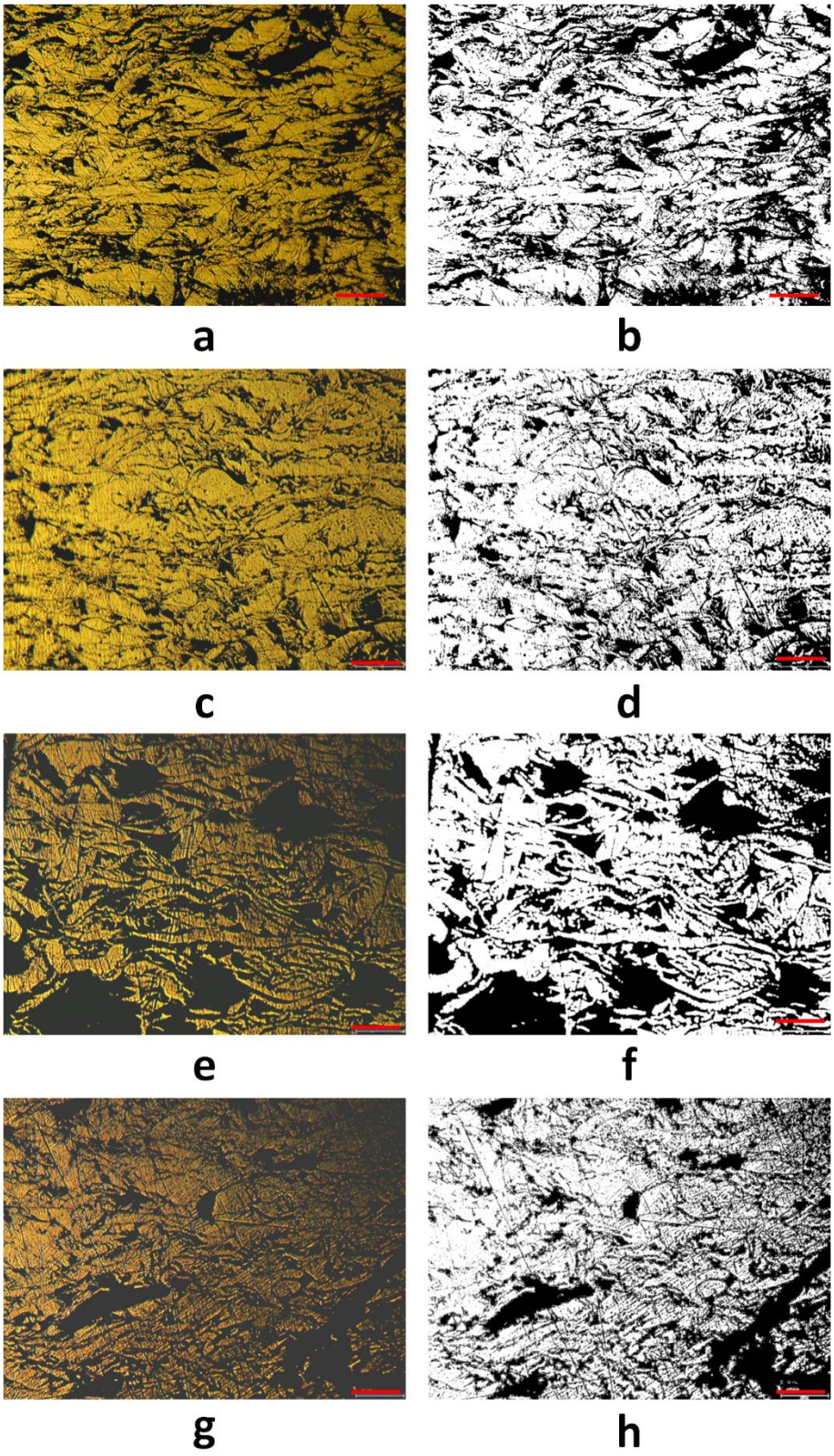

Figure 21. Microscope and processed images for the Mg alloy discs notated as 1(a,b), 3 (c,d), 5 (e,f), and 7 (g,h) (Red colored scale: 200 μm).

3.1.5 Brunauer-Emmett-Teller (BET) Surface Area Analysis

The surface analysis results are depicted in Figure 22. The highest specific surface area (3.55 m^2/g) was measured from as-received Mg alloy powder as expected. The lowest specific surface area (2.83 m^2/g) was found in the Mg alloy disc with a smooth surface. The textured Mg alloy discs which are sintered for 30 and 150 min had a specific surface area of 2.88 and 3.06 m^2/g, respectively. The textured surface disc had higher specific surface area than the one with smooth surface but not as-received powder. According to Figure 22, longer sintering time (150 min) helped to reduce pore size on the surface and the specific surface area decreased. It has been previously mentioned in the literature that longer sintering times are effective to blind pores on the surface by the mechanism of grain growth according to the Hall-Petch relation (Hussein et al., 2015; Li and Yu, 2013; Xu et al., 2013; Yang et al., 2015). The closure of pores was provided by the time so the specific surface area decreased. It was also expected that smooth surface will have lower specific surface area than other samples. The specific surface area data will be used to discuss in terms of biological response of the Mg alloy discs in later paragraphs.

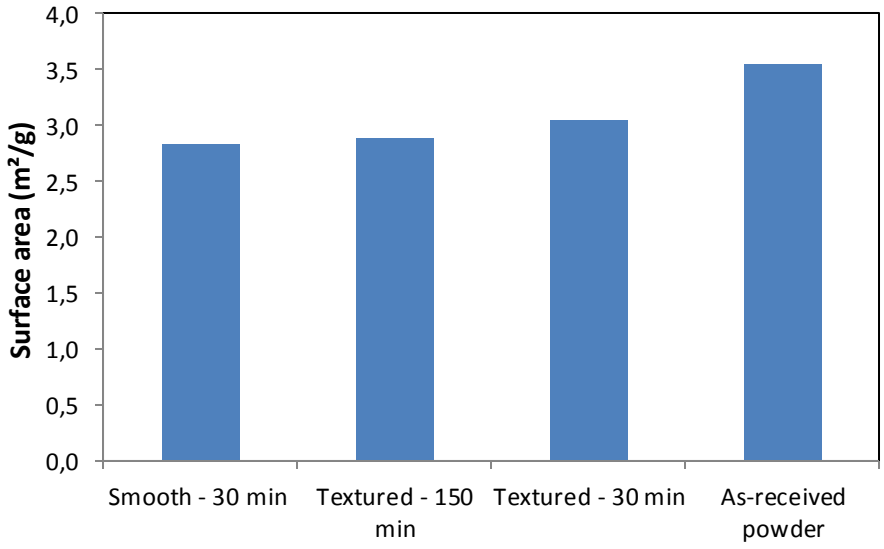

Figure 22. Specific surface area of the selected powder processed and as-received powder samples.

3.2 Mechanical tests

3.2.1 Diametral tensile test

The effect of manufacturing (compaction pressure and sintering time) and surface condition (smooth and textured) on the diametral tensile strength of the Mg alloy discs were evaluated by diametral (or indirect tensile) test. The mechanical integrity is important for the survival of biomedical implants. It is one of the two requirements that an implant should have (Niinomi et al., 2012). An implant has to satisfy biological prerequisites such as biocompability as well as mechanical strength for the sake of safeness during implantation (Niinomi et al., 2012). The 40 MPa compacted Mg alloy powders had an indirect tensile strength of 3.97 and 5.01 MPa. The strength values were reasonable with the values in other experiments in the literature. Metal powders with a relative density up to 80% had a diametral tensile strength of 6.15 MPa at maximum (Jonsén et al., 2007).

As can be seen in Figure 23, an increase in compaction pressure led to an increase in diametral tensile strength. In literature, there is a lack of study on the effect of compaction pressure on the diametral tensile strength. Thus, it is hard to compare the relationship between the diametral tensile strength and compaction pressure. Alternatively, it has been proposed to investigate the relationship between the relative density and the mechanical property rather than compaction pressure in this study. The proposed comparison was applicable because compaction pressure and relative density were almost perfectly proportional to each other. The effect of relative density on the mechanical properties has been intensively investigated for various metal powders. For instance, Mg alloy powders were investigated in terms of mechanical properties as a function of relative density (Li and Zheng, 2013; Wen et al., 2001; Wen et al., 2004; Xia et al., 2013). The variation in the relative densities was caused by the manufacturing conditions as performed in this study. It was found that the yield strength of the powder processed AZ31 Mg alloy powders decreased from 2.26 to 20.55 MPa as porosity decreased from 75 to 60% (Xia et al., 2013). A similar result was obtained in pure Mg compacted at 100 MPa and sintered 500^0C for 2h (Wen et al., 2001). As the porosity (35 to 55%) increased, the compressive strength decreased from 1.8 to 1.3 GPa. At the end, it can be concluded that

compaction pressure had a significant effect even if it was at small levels (25 and 40 MPa) due to the fact that compaction pressure was a dominant factor in reducing porosity as in other studies which is mentioned above.

Surface condition was also effective on the strength. In general, the Mg alloy discs with textured surface showed poor mechanical integrity. Open pores on the surface of the textured surface discs might be the reason of poor strength. It is a well-known fact that pores or sharp edges can act as stress concentrators which decrease the mechanical strength of porous materials (Xia et al., 2013). When it is considered that a tensile stress gradient will form on the surface of the Mg alloy disc, the surface condition will be vital in terms of mechanical integrity. The existence of pores or cracks on the surface affects the mechanical stability of the materials (Aghion and Perez, 2014; Xia et al., 2013). In this study, pores on the surface of textured Mg alloy discs acted as stress concentrators and decreased the diametral tensile strength. This result was a compatible outcome with the relative density. Low relative density or high porosity decreased the diametral tensile strength. Analogically, the existence of pores on the surface where tensile stress existed caused a decrease in the strength. It was observed that open pore structures have a decreasing effect of elastic modulus as well as compressive stress (Mondal et al., 2014).

Sintering time has been regarded as an influential parameter for possible reasons such as precipitation, secondary phase formation or pore elimination. However, sintering time had no significant effect on the diametral tensile strength. Longer sintering times may cause a change in the mechanical properties. In some cases, sintering time might not affect the mechanical properties depending on the formation other phases or precipitation. In literature, it was found that sintering time could not be effective on the mechanical properties. Similar to this study, the flexural and compressive strength did not change much when sintering time changed as many as 12 h (Čapek and Vojtěch, 2014). Yet, sintering for 24 h did cause a significant change in both flexural and compressive strength of pure Mg discs having a porosity in the range of 24-29vol.%. It could be the reason behind poor sintering time effect that shorter sintering times did not cause any meaningful change in the microstructure.

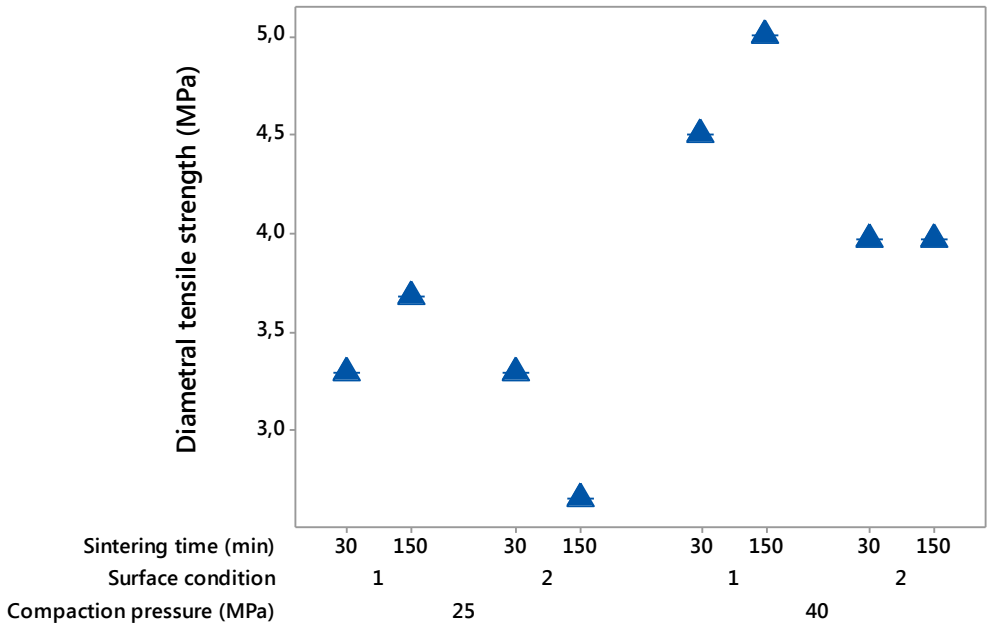

Figure 23. The effect of manufacturing conditions on the diametral tensile strengths of the Mg alloy discs (1: smooth and 2: textured surface).

Apart from relative densities of the Mg alloy discs, the effect of sintering was investigated on the sintered and unsintered discs (Figure 24). The effect of sintering on the mechanical properties of the Mg alloy discs is important because it is expected that sintering causes grain growth and closes pores, which is produced a product with a better mechanical performance. Furthermore, particles bonded to each more strongly during the heat-treatment. Thus, sintering is not only beneficial for pore closure but also increases the bonding strength among particles. These two mechanisms improve the mechanical performance of the unsintered compacts (also referring "green compact"). The sintered discs had an average strength of 3.22 MPa as the unsintered discs had 2.77 MPa. It corresponds to an increase of 16%. This increase is caused by grain growth during sintering as well as stronger bonding between particles than unsintered particles. This result was in a correlation with the relative density values. The same effect was mentioned in the effect of sintering on the relative density before. Overall, sintering had positive effect on the mechanical properties of the discs when it was considered that sintering also increased the relative density of the discs.

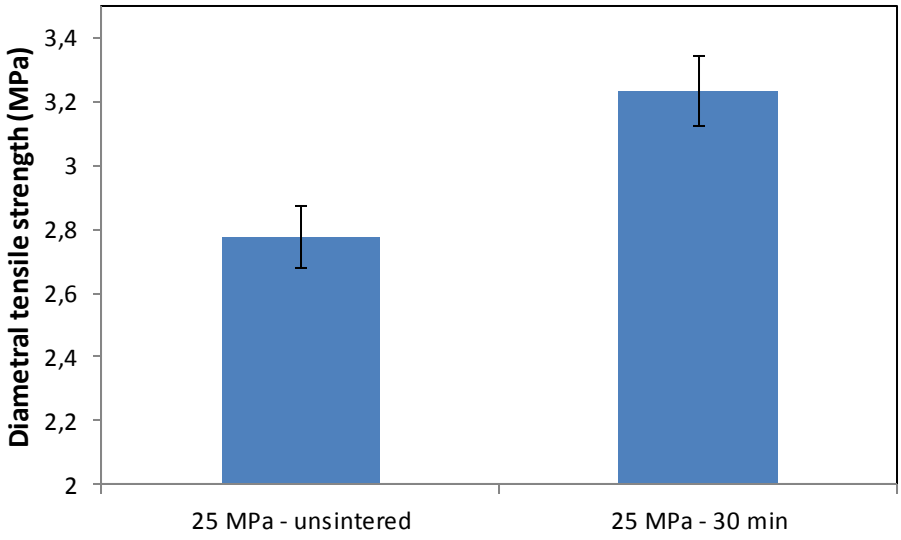

Figure 24. A comparison on the diametral tensile strengths of sintered and unsintered Mg alloy discs.

An image was taken from the surface of the fractured Mg alloy discs (Figure 25). Upper and lower sides of the discs were pressed and flatten during the test. Moreover, continuous cracks from upwards to downwards can be distinctly observed. The cracks were originated from the transformation of compressive forces to tensile forces along the vertical axis. In diametral tensile test, non-linear elastic deformation is followed by linear elastic deformation. At later stages, crack initiates and grows. At the end of the test, cracks widen and become visible as seen in Figure 25. This figure shows the latest stage of the test. Normally, tensile crack is formed in the vertical axis of the discs (Jonsén et al., 2007). There is also a zero stress point on the vertical axis of the disc depending on contact area between sample and pressure applier (Jonsén et al., 2007). Due to the porous structure, tensile cracks were not formed exactly at the vertical axis. Pores at the vertical axis could not bear the compressive stress before compressive stress turned into tensile stress which is perpendicular to the load direction. The upper and lower sides of the discs were squeezed for the same reason.

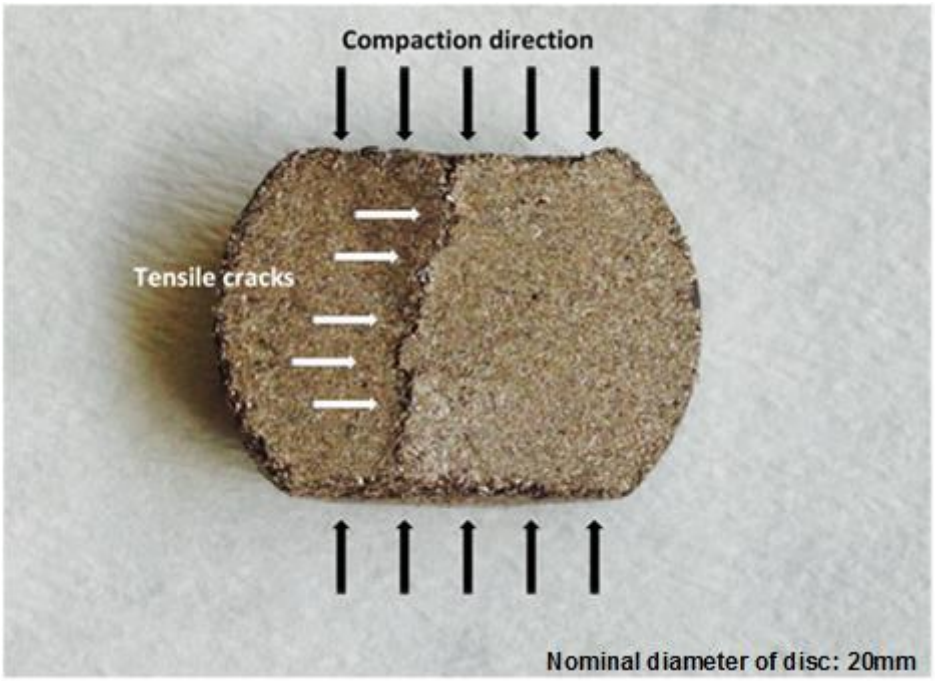

Figure 25. Image of fractured Mg alloy discs in diametral tensile strength.

The fractured surface of the Mg alloy discs (sample 1 and 2) was analyzed by SEM images (Figure 26). It can be seen that the dimples were formed on the surface of the Mg alloy discs. The dimple size suggests some information on the mechanical characteristics of the materials (Evans, 2010; Sabirov et al., 2013). In this study, it was observed that the dimple size reached to 100 μm on the fracture surface. However, this value might be lower than it seems due to the effect of porosity. Already, it can be said that pores may lead an increase in the dimple size. Small dimple size refers to high brittleness (Evans, 2010). The lack of plastic deformation under pressure leads to the formation of small size dimples. In this study, relatively high dimple size was observed than two selected studies that means the Mg alloy discs had a ductile structure even they had a porous structure. Normally, it is expected that porous structures are fractured in a brittle manner (Li and Zheng, 2013). On the contrary, it was seemed that a ductile fracture was observed. However, the needle-like shape, which is thin and long, of the Mg alloy powders might be evaluated as an increasing factor on the ductility.

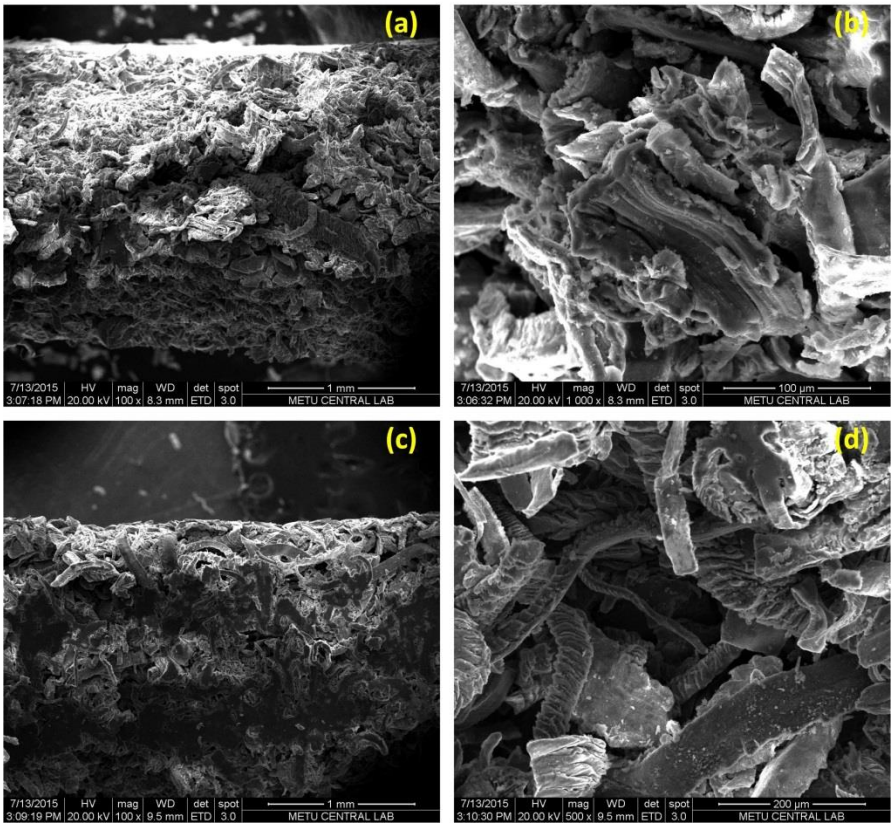

Figure 26. The fractured surfaces of sample 1 (a, b) and 2 (c, d) after diametral tensile test.

3.2.2 Vickers micro-hardness test

The effect of manufacturing conditions on the micro-hardness values is depicted in Figure 27. The micro-hardness values of the discs varied between 13.5 and 84.1 HV. In literature, AZ91D magnesium alloy as bulk material had hardness values of 60-85 HV (Čížek et al., 2004). When it is considered that the Mg alloy discs have a porous structure, it is expected that the hardness values will be lower than that of its bulk counterparts. The hardness of extruded ZK60 Mg alloy had 65-115 HV (Lee et al., 2015). The hardness value of AZ31 Mg alloy was also found between 65 and 85 HV (Xu et al., 2013). It can be concluded that the hardness values of the Mg alloy discs were in acceptable levels.

In Figure 27, sintering time affected the micro-hardness of the Mg alloy discs. In all conditions, the micro-hardness increased as sintering time increased from 30 to 150

min. In general, longer holding at elevated temperature causes grain growth according to the Hall-Petch relation, which is called grain refinement (Li and Yu, 2013). As sintering is in progress of time, particles expand and the contact area among particles increases. Hall-Petch relation suggests that the increase in grain size decreases yield strength of a material. On the other hand, yield strength and hardness have a directly proportional relationship (Li and Yu, 2013). It means that the higher yield strength possess higher hardness values. The results well obeyed this relationship in this study. Moreover, relative density decreased as sintering time increased as stated previously, which also obeys the Hall-Petch relation due to grain growth effect of time. The most dominant mechanism causing an increase in the relative density is grain refinement effect. This effect was investigated by many case studies and the improvement of sintering time on hardness was well-understood. As sintering time increased, the hardness of bulk Ti increased in compatible with relative density (Yang et al., 2015). It was reported that sintering time up to 12 h provided larger grain size of a titania-zirconia-alumina composite which gave improved hardness (Wang and Huang, 2008). Moreover, an improvement (approximately 50%) has been achieved in the hardness of as-casted Mg alloy as sintering time increased from 0 to 12 h (Liang et al., 2014). Thus, the extended sintering time had a positive influence on the micro-hardness values of the discs.

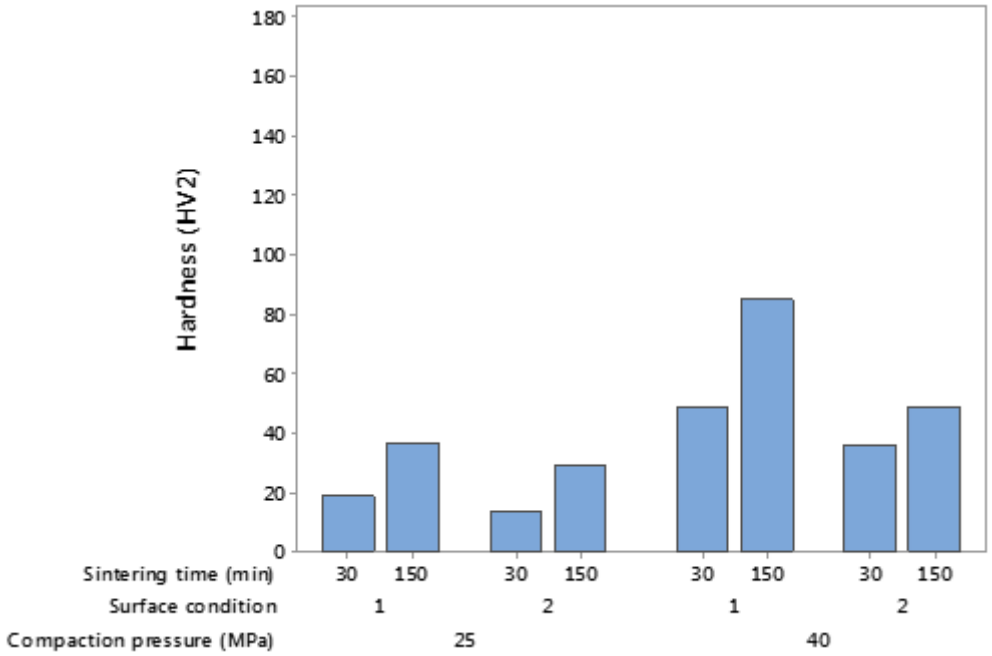

Figure 27. The effect of manufacturing conditions on the hardness of the Mg alloy discs.

However, in some cases, longer sintering times could affect the hardness in a negative manner. A study investigated the effect of sintering time on the hardness and relative density of Nb–Zr alloy for biomedical applications (Hussein et al., 2015). The authors attributed this result to high flux of energy inside the material within these sintering times. The decreasing effect of sintering time was also seen in boron nitride composites manufactured by spark plasma sintering where the micro-hardness reached its minimum as sintering time set as 30 min (Hotta and Goto, 2011). The other reason for negative effect of longer sintering time on the micro-hardness could be originated from the dissolution of the intermetallic or main phases into another main phase as found for Al-CuO composite (Dikici and Gavgali, 2013). In this study, the intermetallic phase intensity decreased after sintering so the positive effect of the sintering time was observed rather than the negative effect. In the light of the literature, sintering has positive or negative effects on the hardness depending on manufacturing conditions and material type. In case sintering causes grain growth obeying Hall-Petch relation, the hardness can be improved as wells as other mechanical properties. The second phase formation or adverse effect of sintering on

grain growth may lead a decrease in hardness. As understood, sintering time points were selected properly and increasing effect of longer sintering time was proved in this study.

Compaction pressure had a direct influence on the micro-hardness of the discs as in the relative density as seen in Figure 27. Regardless of changing other parameters, compaction pressure led to an increase in the micro-hardness values of the discs. The effect of compaction pressure on the micro-hardness as well as the relative density of bulk titanium was investigated (Yang et al., 2015). Furthermore, the effect of compaction pressure on the hardness was proved by several studies (Ibrahim et al., 2015; Srivatsan et al., 2001). The compacted molybdenum and Al alloy powders showed the same hardness characteristic in all compaction pressure levels. The compaction pressure even in small levels (25-40 MPa) had a strong effect on the mechanical properties of the sintered powders.

Surface condition (smooth or textured) did not have an impact to change distinctly the micro-hardness of the discs. The effect of the surface condition was investigated to validate that there is no relationship between surface condition and the micro-hardness.

The formation of diamond-like shape penetration on the surface was observed. A microscope image is be seen in Figure 28. It can be risky to measure hardness from surface of a porous material. Pores can result in an error in micro hardness measurement. Despite porous structure of Mg alloy discs, decent diamond shape was formed on the surface of the discs. In the aforementioned figure, the diagonals of the diamond geometry were measured as 121 and 134 μm.

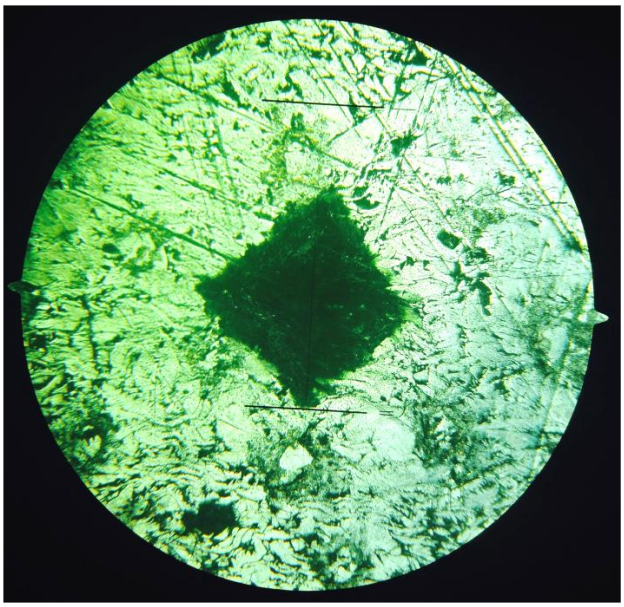

Figure 28. Microscope image of diamond shape penetration on the surface of sample 3

3.3 Computational analysis

Relative densities were numerically analyzed in order to compare with manually calculated relative densities of the Mg alloy discs. Manufacturing conditions were virtually applied in the numerical analysis. In Figure 29.a and b, relative density distribution in the Mg alloy discs compacted under 25 MPa at 150^0C is shown graphically and historiographical. Relative density distribution was distinguished by color. As seen in the image, it could be observed that the density distribution was inhomogeneous and increased toward to the perimeter of the discs. This phenomenon is encountered in many PM products that reduce their mechanical performance. High interparticle friction and low loose powder density are two main reasons of inhomogeneous density distribution in powder compaction (Wolla et al., 2015). Inhomogeneous distribution originates from that the direction compaction force changes into vertical direction through die wall that causes stress increase in the region close to die wall (Al-Qureshi et al., 2008). It is a general tendency in powder compaction that was proved theoretically and experimentally in some studies (Diarra et al., 2012; Kadiri et al., 2005; Wu and Kim, 2011). The same densification profile was observed in this study as compatible with the literature. Besides, it was reported that densification starts from upper part of metal powders regardless of compaction temperature (Güner et al., 2015; Khoei et al., 2012; Rossi et al., 2007). Compaction

pressure led to an increase in the relative density. The average relative density of the 25 MPa compacted discs was 58.8%. The minimum density was 38.7% while the maximum value was 100%.

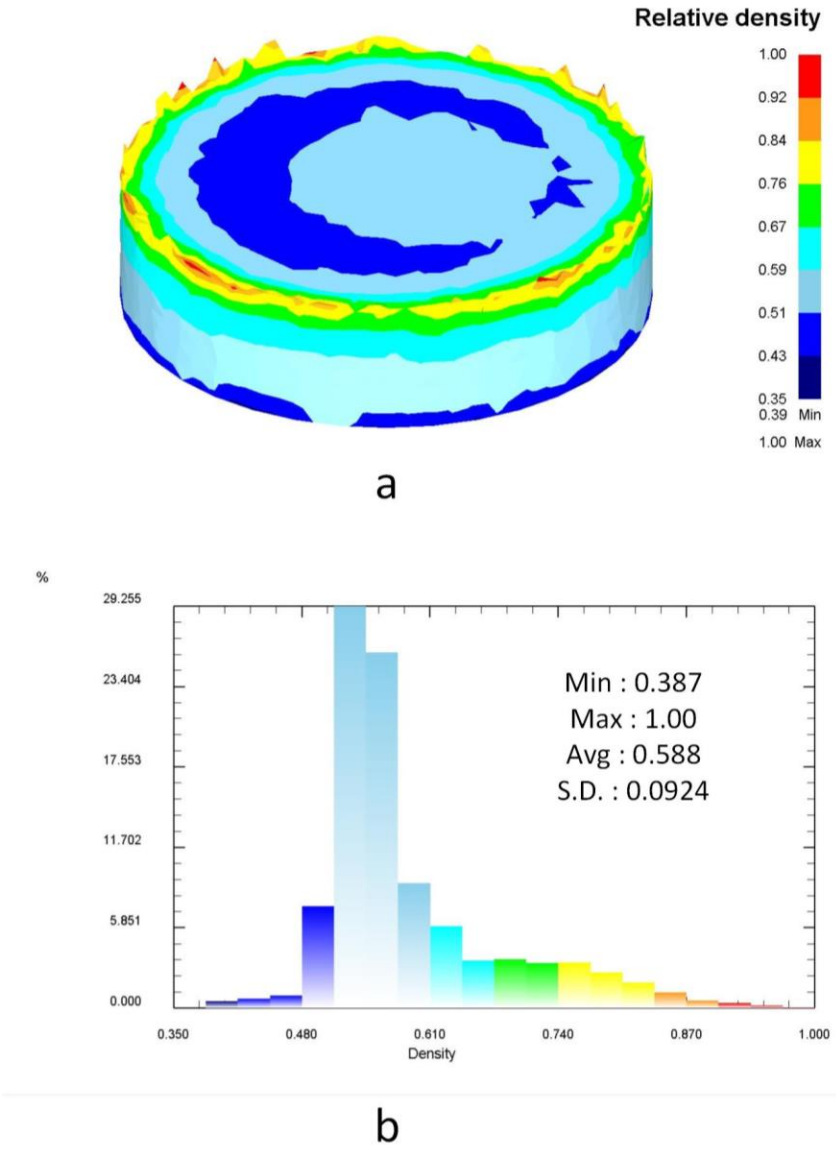

Figure 29. Schematic and histographic representation of relative density distribution.

Numerical and experimental results of relative density are compared to realize the reliability of the numerical prediction. Experimental results were collected from at

least three Mg alloy discs that are manufactured at the same condition. The relative densities of the 25 MPa compacted at 150^0C Mg alloy discs were manually calculated as a percentage of 56.9±0.0091, which is close to the value in computational analysis (58.8%). The results were well matched with manually-calculated relative density values. Mg alloy discs were densified at the same rates in both experimental condition and numerical simulation. These results possessed that material model was created compatible with experimental conditions.

3.4 Cell viability

Figure 30 shows relative viability (with respect to positive control) of hFOB cells seeded on the powder processed Mg alloy discs. Positive control was used to compare the cell viability. The selected Mg alloy discs with smooth and textured surfaces (sample 1 and 3) were exposed to the MTT assay. Sample 1 and 3 were compacted under 40 MPa and sintered for 150^0C. These Mg alloy discs had the highest diametral tensile strength which is important for mechanical integrity. Additionally, the hardness values of these discs were higher in all samples. Moreover, their relative densities were in a reasonable range (0.63-0.65) for cell attachment, spreading and proliferation. Sample 1 and 3 were selected because their mechanical integrity was higher and porosity levels were more suitable for a good biological response. More importantly, high hardness has a promotive effect of osteoblasts cells because these cells more likely proliferate on a harder surface than on a softer one. As it was shown earlier in Table 4, the composition of AZ91D Mg alloy consists of Mg, Al, Zn, Mn and other trace amounts of elements (Ni and Cu). It is known that some elements have toxic or allergenic effects on a living environment (Chen et al., 2014). Elements in the composition such as Mg, Zn and Mn are nutrient elements found in the human body, animals and plants (Chen et al., 2014). Thus, their negative effect can be negligible. Although Al exists in animals and plants, it is probable to show toxic or allergenic effect in case of excessive concentrations. MTT assay was conducted to evaluate the possible effect of these elements.

Initial mechanisms are cell adhesion, spreading and migration when cells are seeded on a material surface (Li et al., 2014). MTT assay gives a perspective on possible toxic effects of materials. According to ISO 10993-5:2009, the death cell ratio more than 30% means that the material is not biocompatible for that cells which is seeded (Li and Zheng, 2013). In this study, the hFOB cells which is seeded on both samples showed an increasing tendency as incubation time was reached to 4 and 7 days. In any time point, the viability did not decrease. It implies that the used material is a biocompatible material for hFOB cells.

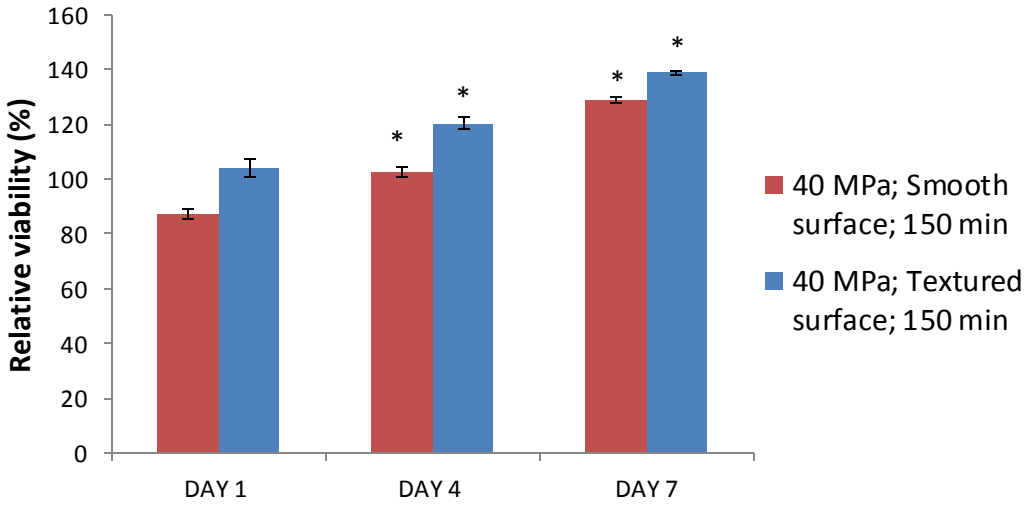

Figure 30. hFOB cell growth assessment on the Mg alloy discs by MTT viability test (Statistical significance from the positive control at $p < 0.05$ is presented as *).

In this study, the assumption is that an implant surface can be improved via powder metallurgy in combination with micro-manufacturing by producing a non-smooth surface rather than a smooth one. It is a well-recognized fact that rough surfaces are able to increase the bonding between implant and bone through increasing osseointegration (Pompa et al., 2015). According to the BET analysis, the Mg alloy discs with a textured surface had a higher specific surface area (3.06 and 2.88 m^2/g) than the discs with smooth one (2.83 m^2/g). The Mg alloy disc with a rough surface (sample 4) had higher viability values than the smooth one (sample 2) as parallel to BET analysis results. It has been tried to manufacture a hierarchical surface structure like lotus-type porous surface that it has characteristic of micro or nano structures on

greater micro structures. It was proved that this kind of a surface decreased the H_2 gas evaluation and mass loss (Gu et al., 2010). It is considered that excessive H_2 gas evolution increases osmotic pressure and causes the death of cells (Gu et al., 2010). The higher cell viability on the textured surface could be related to preservative effect of rough surface from high gas evolution.

CHAPTER 4

CONCLUSIONS

In this study, Mg alloy discs with smooth and textured surfaces were manufactured by PM in order to investigate their microstructural, mechanical and biological properties. The AZ91D Mg alloy powders were compacted under 25 and 40 MPa at 150°C. All samples were then sintered at 380°C for 30 and 150 min to distinguish the effect of sintering time on the relative density, diametral tensile strength and Vickers micro hardness. Moreover, the sintered and unsintered discs were compared in terms of the relative densities and diametral tensile strengths in order to assess the effect of sintering process.

Compaction pressure was a dominant factor in all material properties studied in this work. The increase in compaction pressure increased the relative density, diametral tensile strength and Vickers hardness of the Mg alloy discs. Sintering time did not influence the relative densities and the diametral tensile strength of the samples. However, Vickers hardness values increased significantly as sintering time lasted. Although surface condition was employed to characterize with biological concerns, the effect of the surface condition on the physical and mechanical properties was also evaluated. The smooth surfaces had lower relative densities than the textured surfaces. Apart from this, surface condition did not affect material properties of the discs. Moreover, the sintered and unsintered discs were evaluated in order to distinguish the effect of sintering process. Under all circumstances, the sintered discs had better physical and mechanical properties.

Compaction stage (25 MPa and 150^{0}C) was simulated in a software by implementing process parameters. The experimental and computational results were compared and well matched. Moreover, SEM images were converted to black/white images to predict the relative density of the discs. Manually-calculated relative densities and image processing results were in a good agreement.

Microstructural evaluation was conducted to observe porous nature inside the discs via light and scanning electron microscopy. Pores were identified in the dimension up to 100 μm. Surface analyses showed that the textured surface had more specific area than the smooth surfaces. Furthermore, the fractured surfaces after the diametral tensile test were analyzed through SEM images and evaluated.

The biological response of the Mg alloy discs to hFOB cells was in a good manner. The discs showed no toxicity with increasing the relative cell viability. Textured surfaces were also better at cell adhesion, growth and proliferation according to MTT assay results.

REFERENCES

Aghion, E., Perez, Y., 2014. Effects of porosity on corrosion resistance of Mg alloy foam produced by powder metallurgy technology. Materials Characterization 96, 78-83.

Al-Qureshi, H., Soares, M., Hotza, D., Alves, M., Klein, A., 2008. Analyses of the fundamental parameters of cold die compaction of powder metallurgy. Journal of Materials Processing Technology 199, 417-424.

Arifin, A., Sulong, A.B., Muhamad, N., Syarif, J., Ramli, M.I., 2014. Material processing of hydroxyapatite and titanium alloy (HA/Ti) composite as implant materials using powder metallurgy: a review. Materials & Design 55, 165-175.

Askeland, D., Fulay, P., Wright, W., 2011. The Science and Engineering of Materials, 6th Edition ed. Cengage Learning, USA.

ASTM Standard B 93/B 93M, 1990.

Babakhani, A., Haerian, A., Ghambari, M., 2006. On the combined effect of lubrication and compaction temperature on properties of iron-based P/M parts. Materials Science and Engineering: A 437, 360-365.

Bakhsheshi-Rad, H., Idris, M., Abdul-Kadir, M., Ourdjini, A., Medraj, M., Daroonparvar, M., Hamzah, E., 2014. Mechanical and bio-corrosion properties of quaternary Mg–Ca–Mn–Zn alloys compared with binary Mg–Ca alloys. Materials & Design 53, 283-292.

Bartolo, P., Kruth, J.-P., Silva, J., Levy, G., Malshe, A., Rajurkar, K., Mitsuishi, M., Ciurana, J., Leu, M., 2012. Biomedical production of implants by additive electro-

chemical and physical processes. CIRP Annals-Manufacturing Technology 61, 635-655.

Bauer, S., Schmuki, P., von der Mark, K., Park, J., 2013. Engineering biocompatible implant surfaces: Part I: Materials and surfaces. Progress in Materials Science 58, 261-326.

Boland, C., Hexemer Jr, R., Donaldson, I., Bishop, D., 2013. Industrial processing of a novel Al–Cu–Mg powder metallurgy alloy. Materials Science and Engineering: A 559, 902-908.

Bolzoni, L., Ruiz-Navas, E.M., Gordo, E., 2013. Influence of sintering parameters on the properties of powder metallurgy Ti–3Al–2.5 V alloy. Materials Characterization 84, 48-57.

Brånemark, R., Emanuelsson, L., Palmquist, A., Thomsen, P., 2011. Bone response to laser-induced micro-and nano-size titanium surface features. Nanomedicine: Nanotechnology, Biology and Medicine 7, 220-227.

Brar, H.S., Wong, J., Manuel, M.V., 2012. Investigation of the mechanical and degradation properties of Mg–Sr and Mg–Zn–Sr alloys for use as potential biodegradable implant materials. Journal of the Mechanical Behavior of Biomedical Materials 7, 87-95.

Čapek, J., Vojtěch, D., 2014. Effect of sintering conditions on the microstructural and mechanical characteristics of porous magnesium materials prepared by powder metallurgy. Materials Science and Engineering: C 35, 21-28.

Castellani, C., Lindtner, R.A., Hausbrandt, P., Tschegg, E., Stanzl-Tschegg, S.E., Zanoni, G., Beck, S., Weinberg, A.-M., 2011. Bone–implant interface strength and

osseointegration: biodegradable magnesium alloy versus standard titanium control. Acta Biomaterialia 7, 432-440.

Chen, W., Yamamoto, Y., Peter, W.H., Gorti, S.B., Sabau, A.S., Clark, M.B., Nunn, S.D., Kiggans, J., Blue, C.A., Williams, J., 2011. Cold compaction study of Armstrong process Ti–6Al–4V powders. Powder Technology 214, 194-199.

Chen, Y., Xu, Z., Smith, C., Sankar, J., 2014. Recent advances on the development of magnesium alloys for biodegradable implants. Acta Biomaterialia 10, 4561-4573.

Chu, Q., Liang, J., Hao, J., 2014. Facile fabrication of a robust super-hydrophobic surface on magnesium alloy. Colloids and Surfaces A: Physicochemical and Engineering Aspects 443, 118-122.

Čížek, L., Greger, M., Pawlica, L., Dobrzański, L.A., Tański, T., 2004. Study of selected properties of magnesium alloy AZ91 after heat treatment and forming. Journal of Materials Processing Technology 157, 466-471.

Dahle, A.K., Lee, Y.C., Nave, M.D., Schaffer, P.L., John, D.H., 2001. Development of the as-cast microstructure in magnesium–aluminium alloys. Journal of Light Metals 1, 61-72.

Dám, K., Vojtěch, D., Průša, F., 2013. Powder metallurgy Al–6Cr–2Fe–1Ti alloy prepared by melt atomisation and hot ultra-high pressure compaction. Materials Science and Engineering: A 560, 705-710.

Della Bona, Á., Benetti, P., Borba, M., Cecchetti, D., 2008. Flexural and diametral tensile strength of composite resins. Brazilian Oral Research 22, 84-89.

Denkena, B., Lucas, A., 2007. Biocompatible magnesium alloys as absorbable implant materials–adjusted surface and subsurface properties by machining processes. CIRP Annals-Manufacturing Technology 56, 113-116.

Diarra, H., Mazel, V., Boillon, A., Rehault, L., Busignies, V., Bureau, S., Tchoreloff, P., 2012. Finite element method (FEM) modeling of the powder compaction of cosmetic products: Comparison between simulated and experimental results. Powder Technology 224, 233-240.

Dikici, B., Gavgali, M., 2013. The effect of sintering time on synthesis of in situ submicron α-Al2O3 particles by the exothermic reactions of CuO particles in molten pure Al. Journal of Alloys and Compounds 551, 101-107.

Dorozhkin, S.V., 2014. Calcium orthophosphate coatings on magnesium and its biodegradable alloys. Acta Biomaterialia 10, 2919-2934.

Du, H., Wei, Z., Liu, X., Zhang, E., 2011. Effects of Zn on the microstructure, mechanical property and bio-corrosion property of Mg–3Ca alloys for biomedical application. Materials Chemistry and Physics 125, 568-575.

Duan, H., Han, G., Wang, M., Zhang, X., Liu, Z., Liu, Z., 2014. Rotation friction pressing riveting of AZ31 magnesium alloy sheet. Materials & Design 54, 414-424.

Dudek, A., Włodarczyk, R., 2013. Effect of sintering atmosphere on properties of porous stainless steel for biomedical applications. Materials Science and Engineering: C 33, 434-439.

Enneti, R.K., Lusin, A., Kumar, S., German, R.M., Atre, S.V., 2013. Effects of lubricant on green strength, compressibility and ejection of parts in die compaction process. Powder Technology 233, 22-29.

Evans, J.L., 2010. Thermal history and tensile strength determination from fracture surface analysis. Engineering Failure Analysis 17, 882-885.

Fan, T.-W., Zhang, Q., Ma, L., Tang, P.-Y., Tang, B.-Y., Peng, L.-M., Ding, W.-J., 2014. First-principles study of the dislocation core structures on basal plane in magnesium. European Journal of Mechanics-A/Solids 45, 1-7.

Fedrizzi, A., Pellizzari, M., Zadra, M., 2012. Influence of particle size ratio on densification behaviour of AISI H13/AISI M3:2 powder mixture. Powder Technology 228, 435-442.

Ferreira, M.E., Pereira, M.D.L., Sousa, J.P., Simões de Carvalho, G., 2003. Comparative study of metallic biomaterials toxicity: a histochemical and immunohistochemical demonstration in mouse spleen. Journal of Trace Elements in Medicine and Biology 17, 45-49.

Fu, G., Soboyejo, W., 2009. Cell/surface interactions of human osteo-sarcoma (HOS) cells and micro-patterned polydimelthylsiloxane (PDMS) surfaces. Materials Science and Engineering: C 29, 2011-2018.

Garg, P., Park, S.-J., German, R.M., 2007. Effect of die compaction pressure on densification behavior of molybdenum powders. International Journal of Refractory Metals and Hard Materials 25, 16-24.

Geis-Gerstorfer, J., Schille, C., Schweizer, E., Rupp, F., Scheideler, L., Reichel, H., Hort, N., Nolte, A., Wendel, H., 2011. Blood triggered corrosion of magnesium alloys. Materials Science and Engineering: B 176, 1761-1766.

German, R.M., 2005. Powder metallurgy and particulate materials processing, 1st Edition ed. Metal Powder Industries Federation Princeton, NJ.

Gu, X., Zhou, W., Zheng, Y., Liu, Y., Li, Y., 2010. Degradation and cytotoxicity of lotus-type porous pure magnesium as potential tissue engineering scaffold material. Materials Letters 64, 1871-1874.

Gu, X.-N., Zheng, Y.-F., 2010. A review on magnesium alloys as biodegradable materials. Frontiers of Materials Science in China 4, 111-115.

Güner, F., Cora, Ö.N., Sofuoğlu, H., 2015. Numerical modeling of cold powder compaction using multi particle and continuum media approaches. Powder Technology 271, 238-247.

Guo, Y., Salahshoor, M., 2010. Process mechanics and surface integrity by high-speed dry milling of biodegradable magnesium–calcium implant alloys. CIRP Annals-Manufacturing Technology 59, 151-154.

Gzyl, M., Rosochowski, A., Boczkal, S., Olejnik, L., 2015. The role of microstructure and texture in controlling mechanical properties of AZ31B magnesium alloy processed by I-ECAP. Materials Science and Engineering: A 638, 20-29.

Haase, K., Rouhi, G., 2013. Prediction of stress shielding around an orthopedic screw: Using stress and strain energy density as mechanical stimuli. Computers in Biology and Medicine 43, 1748-1757.

Harandi, S.E., Hasbullah Idris, M., Jafari, H., 2011. Effect of forging process on microstructure, mechanical and corrosion properties of biodegradable Mg–1Ca alloy. Materials & Design 32, 2596-2603.

Haugen, H.J., Monjo, M., Rubert, M., Verket, A., Lyngstadaas, S.P., Ellingsen, J.E., Rønold, H.J., Wohlfahrt, J.C., 2013. Porous ceramic titanium dioxide scaffolds

promote bone formation in rabbit peri-implant cortical defect model. Acta Biomaterialia 9, 5390-5399.

Hermawan, H., Dubé, D., Mantovani, D., 2010. Developments in metallic biodegradable stents. Acta Biomaterialia 6, 1693-1697.

Holzapfel, B.M., Reichert, J.C., Schantz, J.-T., Gbureck, U., Rackwitz, L., Noeth, U., Jakob, F., Rudert, M., Groll, J., Hutmacher, D.W., 2013. How smart do biomaterials need to be? A translational science and clinical point of view. Advanced Drug Delivery Reviews 65, 581-603.

Homayun, B., Afshar, A., 2014. Microstructure, mechanical properties, corrosion behavior and cytotoxicity of Mg–Zn–Al–Ca alloys as biodegradable materials. Journal of Alloys and Compounds 607, 1-10.

Hornberger, H., Virtanen, S., Boccaccini, A., 2012. Biomedical coatings on magnesium alloys–A review. Acta Biomaterialia 8, 2442-2455.

Hort, N., Huang, Y., Fechner, D., Störmer, M., Blawert, C., Witte, F., Vogt, C., Drücker, H., Willumeit, R., Kainer, K., 2010. Magnesium alloys as implant materials–Principles of property design for Mg–RE alloys. Acta Biomaterialia 6, 1714-1725.

Hotta, M., Goto, T., 2011. Effect of time on microstructure and hardness of βSiAlON–cubic boron nitride composites during spark plasma sintering. Ceramics International 37, 521-524.

Hsu, H.-C., Wu, S.-C., Hsu, S.-K., Chang, T.-Y., Ho, W.-F., 2014. Effect of ball milling on properties of porous Ti–7.5 Mo alloy for biomedical applications. Journal of Alloys and Compounds 582, 793-801.

Huang, S.-H., Lin, L.-S., Fok, A.S., Lin, C.-P., 2012a. Diametral compression test with composite disk for dentin bond strength measurement–Finite element analysis. Dental Materials 28, 1098-1104.

Huang, S.-H., Lin, L.-S., Rudney, J., Jones, R., Aparicio, C., Lin, C.-P., Fok, A., 2012b. A novel dentin bond strength measurement technique using a composite disk in diametral compression. Acta Biomaterialia 8, 1597-1602.

Hussein, M., Suryanarayana, C., Arumugam, M., Al-Aqeeli, N., 2015. Effect of sintering parameters on microstructure, mechanical properties and electrochemical behavior of Nb–Zr alloy for biomedical applications. Materials & Design 83, 344-351.

Ibrahim, A., Bishop, D.P., Kipouros, G.J., 2015. Sinterability and characterization of commercial aluminum powder metallurgy alloy Alumix 321. Powder Technology 279, 106-112.

Jabur, A.S., 2013. Effect of powder metallurgy conditions on the properties of porous bronze. Powder Technology 237, 477-483.

Jeong, J.H., Ryu, S.K., Park, S.J., Shin, H.C., Yu, J.H., 2015. Analysis of iron powder design for compaction process. Computational Materials Science 100, 21-30.

Jeong, M.-S., Yoo, J.-H., Rhim, S.-H., Lee, S.-K., Oh, S.-I., 2012. A unified model for compaction and sintering behavior of powder processing. Finite Elements in Analysis and Design 53, 56-62.

Jonsén, P., Häggblad, H.-Å., Sommer, K., 2007. Tensile strength and fracture energy of pressed metal powder by diametral compression test. Powder Technology 176, 148-155.

Kadiri, M., Michrafy, A., Dodds, J., 2005. Pharmaceutical powders compaction: experimental and numerical analysis of the density distribution. Powder Technology 157, 176-182.

Kaiser, R., Williamson, K., O'Brien, C., Ramirez-Garcia, S., Browne, D., 2013. The influence of cooling conditions on grain size, secondary phase precipitates and mechanical properties of biomedical alloy specimens produced by investment casting. Journal of the Mechanical Behavior of Biomedical Materials 24, 53-63.

Kang, C.S., Lee, S., Kim, K., Rozenberg, O., 2007. Densification behavior of iron powder during cold stepped compaction. Materials Science and Engineering: A 452, 359-366.

Khoei, A., Biabanaki, S., Parvaneh, S., 2012. Dynamic modeling of powder compaction processes via a simple contact algorithm. International Journal of Mechanical Sciences 64, 196-210.

Klocke, F., Schwade, M., Klink, A., Veselovac, D., Kopp, A., 2013. Influence of electro discharge machining of biodegradable magnesium on the biocompatibility. Procedia CIRP 5, 88-93.

Kurgan, N., 2014. Effect of porosity and density on the mechanical and microstructural properties of sintered 316L stainless steel implant materials. Materials & Design 55, 235-241.

Kurgan, N., Varol, R., 2010. Mechanical properties of P/M 316L stainless steel materials. Powder Technology 201, 242-247.

Lee, H.-J., Lee, S.K., Jung, K.H., Lee, G.A., Ahn, B., Kawasaki, M., Langdon, T.G., 2015. Evolution in hardness and texture of a ZK60A magnesium alloy processed by high-pressure torsion. Materials Science and Engineering: A 630, 90-98.

Li, C., Yu, Y.D., 2013. The effect of solution heat treatments on the microstructure and hardness of ZK60 magnesium alloys prepared under low-frequency alternating magnetic fields. Materials Science and Engineering: A 559, 22-28.

Li, M., Ren, L., Li, L., He, P., Lan, G., Zhang, Y., Yang, K., 2014. Cytotoxic effect on osteosarcoma MG-63 cells by degradation of magnesium. Journal of Materials Science & Technology 30, 888-893.

Li, N., Zheng, Y., 2013. Novel magnesium alloys developed for biomedical application: A review. Journal of Materials Science & Technology 29, 489-502.

Liang, C., Liu, W.-C., Li, Z.-Q., Wu, G.-H., Lu, X., Wang, S.-H., Ding, W.-J., 2014. Effect of heat treatment on microstructures and mechanical properties of sand-cast Mg-10Gd-3Y-0.5 Zr magnesium alloy. Transactions of Nonferrous Metals Society of China 24, 611-618.

Liu, C., Shi, B., Zhou, J., Tang, C., 2011. Quantification and characterization of microporosity by image processing, geometric measurement and statistical methods: Application on SEM images of clay materials. Applied Clay Science 54, 97-106.

Liu, C., Yang, H., Wan, P., Wang, K., Tan, L., Yang, K., 2014. Study on biodegradation of the second phase Mg17Al12 in Mg–Al–Zn Alloys: In vitro experiment and thermodynamic calculation. Materials Science and Engineering: C 35, 1-7.

Lu, Y., Tan, L., Zhang, B., Lin, J., Yang, K., 2014. Synthesis and characterization of Ca–Sr–P coating on pure magnesium for biomedical application. Ceramics International 40, 4559-4565.

Maru, M., Amaral, M., Rodrigues, S., Santos, R., Gouvea, C., Archanjo, B., Trommer, R., Oliveira, F., Silva, R., Achete, C., 2015. The High performance of

nanocrystalline CVD diamond coated hip joints in wear simulator test. Journal of the Mechanical Behavior of Biomedical Materials.

Mastai, Y, 2013. Materials Science - Advanced Topics, 1st Ed. InTech, USA.

Mazraeshahi, E.M., Nami, B., Miresmaeili, S., Tabatabaei, S., 2015. Effect of Si on the creep properties of AZ61 cast magnesium alloy. Materials & Design 76, 64-70.

Mazzoli, A., Favoni, O., 2012. Particle size, size distribution and morphological evaluation of airborne dust particles of diverse woods by scanning electron microscopy and image processing program. Powder Technology 225, 65-71.

Mirhosseini, N., Crouse, P., Schmidth, M., Li, L., Garrod, D., 2007. Laser surface micro-texturing of Ti–6Al–4V substrates for improved cell integration. Applied Surface Science 253, 7738-7743.

Mondal, D., Patel, M., Das, S., Jha, A., Jain, H., Gupta, G., Arya, S., 2014. Titanium foam with coarser cell size and wide range of porosity using different types of evaporative space holders through powder metallurgy route. Materials & Design 63, 89-99.

Moravej, M., Mantovani, D., 2011. Biodegradable metals for cardiovascular stent application: Interests and new opportunities. International Journal of Molecular Sciences 12, 4250-4270.

Narayanan, T.S., Park, I.S., Lee, M.H., 2014. Strategies to improve the corrosion resistance of microarc oxidation (MAO) coated magnesium alloys for degradable implants: Prospects and challenges. Progress in Materials Science 60, 1-71.

Niinomi, M., 2007. Fatigue characteristics of metallic biomaterials. International Journal of Fatigue 29, 992-1000.

Niinomi, M., Nakai, M., Hieda, J., 2012. Development of new metallic alloys for biomedical applications. Acta Biomaterialia 8, 3888-3903.

Nor, S., Rahman, M., Tarlochan, F., Shahida, B., Ariffin, A., 2008. The effect of lubrication in reducing net friction in warm powder compaction process. Journal of Materials Processing Technology 207, 118-124.

Okulov, I., Pauly, S., Kühn, U., Gargarella, P., Marr, T., Freudenberger, J., Schultz, L., Scharnweber, J., Oertel, C.-G., Skrotzki, W., 2013. Effect of microstructure on the mechanical properties of as-cast Ti–Nb–Al–Cu–Ni alloys for biomedical application. Materials Science and Engineering: C 33, 4795-4801.

Omidi, S., Bahmani Oskooee, M., 2013. Analysis of stress concentration in bone–implant interface using different shapes of the implant: Porous Ti and ultra-fine grained Ti. Indian Journal of Dentistry 4, 125-128.

Palanivelu, R., Kalainathan, S., Kumar, A.R., 2014. Characterization studies on plasma sprayed (AT/HA) bi-layered nano ceramics coating on biomedical commercially pure titanium dental implant. Ceramics International 40, 7745-7751.

Peng, Q., Li, X., Ma, N., Liu, R., Zhang, H., 2012. Effects of backward extrusion on mechanical and degradation properties of Mg–Zn biomaterial. Journal of the Mechanical Behavior of Biomedical Materials 10, 128-137.

Pizette, P., Martin, C., Delette, G., Sornay, P., Sans, F., 2010. Compaction of aggregated ceramic powders: From contact laws to fracture and yield surfaces. Powder Technology 198, 240-250.

Pompa, L., Rahman, Z.U., Munoz, E., Haider, W., 2015. Surface characterization and cytotoxicity response of biodegradable magnesium alloys. Materials Science and Engineering: C 49, 761-768.

Poquillon, D., Lemaitre, J., Baco-Carles, V., Tailhades, P., Lacaze, J., 2002. Cold compaction of iron powders—relations between powder morphology and mechanical properties: Part I: Powder preparation and compaction. Powder Technology 126, 65-74.

Purnama, A., Hermawan, H., Mantovani, D., 2014. Biodegradable metal stents: A focused review on materials and clinical studies. Journal of Biomaterials and Tissue Engineering 4, 868-874.

Rahimian, M., Ehsani, N., Parvin, N., 2009. The effect of particle size, sintering temperature and sintering time on the properties of Al–Al2O3 composites, made by powder metallurgy. Journal of Materials Processing Technology 209, 5387-5393.

Ren, L., Yang, K., 2013. Bio-functional design for metal implants, a new concept for development of metallic biomaterials. Journal of Materials Science & Technology 29, 1005-1010.

Ringoir, S., Vanholder, R., 1986. An introduction to biocompatibility. Artificial Organs 10, 20-27.

Rojaee, R., Fathi, M., Raeissi, K., 2013. Electrophoretic deposition of nanostructured hydroxyapatite coating on AZ91 magnesium alloy implants with different surface treatments. Applied Surface Science 285, 664-673.

Rosengren, Å., Pavlovic, E., Oscarsson, S., Krajewski, A., Ravaglioli, A., Piancastelli, A., 2002. Plasma protein adsorption pattern on characterized ceramic biomaterials. Biomaterials 23, 1237-1247.

Rossi, R., Alves, M., Al-Qureshi, H., 2007. A model for the simulation of powder compaction processes. Journal of Materials Processing Technology 182, 286-296.

Rothen-Weinhold, A., Besseghir, K., Vuaridel, E., Sublet, E., Oudry, N., Kubel, F., Gurny, R., 1999. Injection-molding versus extrusion as manufacturing technique for the preparation of biodegradable implants. European Journal of Pharmaceutics and Biopharmaceutics 48, 113-121.

Sabirov, I., Valiev, R., Pippan, R., 2013. About application of three dimensional analyses of fracture surfaces in fracture study on nanostructured titanium. Computational Materials Science 76, 72-79.

Saha, B.P., Kumar, V., Joshi, S.V., Balakrishnan, A., Martin, C.L., 2012. Investigation of compaction behavior of alumina nano powder. Powder Technology 224, 90-95.

Salahshoor, M., Guo, Y., 2011. Surface integrity of biodegradable orthopedic magnesium–calcium alloy by high-speed dry face milling. Production Engineering 5, 641-650.

Seyedraoufi, Z., Mirdamadi, S., 2013. Synthesis, microstructure and mechanical properties of porous Mg-Zn scaffolds. Journal of the Mechanical Behavior of Biomedical Materials 21, 1-8.

Shukla, A., Narayana Murty, S., Suresh Kumar, R., Mondal, K., 2012. Densification behavior and mechanical properties of Cu–Cr–Nb alloy powders. Materials Science and Engineering: A 551, 241-248.

Simchi, A., 2003. Effects of lubrication procedure on the consolidation, sintering and microstructural features of powder compacts. Materials & Design 24, 585-594.

Smith, L., Midha, P., Graham, A., 1998. Simulation of metal powder compaction, for the development of a knowledge based powder metallurgy process advisor. Journal of Materials Processing Technology 79, 94-100.

Song, Y., Shan, D., Chen, R., Zhang, F., Han, E.-H., 2009. Biodegradable behaviors of AZ31 magnesium alloy in simulated body fluid. Materials Science and Engineering: C 29, 1039-1045.

Souto, P., Camerucci, M., Martinez, A.T., Kiminami, R., 2011. High-temperature diametral compression strength of microwave-sintered mullite. Journal of the European Ceramic Society 31, 2819-2826.

Srinivasan, A., Pillai, U., Pai, B., 2010. Effects of elemental additions (Si and Sb) on the ageing behavior of AZ91 magnesium alloy. Materials Science and Engineering: A 527, 6543-6550.

Srivatsan, T., Ravi, B., Naruka, A., Riester, L., Petraroli, M., Sudarshan, T., 2001. The microstructure and hardness of molybdenum powders consolidated by plasma pressure compaction. Powder Technology 114, 136-144.

Staiger, M.P., Kolbeinsson, I., Kirkland, N.T., Nguyen, T., Dias, G., Woodfield, T.B., 2010. Synthesis of topologically-ordered open-cell porous magnesium. Materials Letters 64, 2572-2574.

Staiger, M.P., Pietak, A.M., Huadmai, J., Dias, G., 2006. Magnesium and its alloys as orthopedic biomaterials: A review. Biomaterials 27, 1728-1734.

Staišiūnas, L., Miečinskas, P., Leinartas, K., Selskis, A., Grigucevičienė, A., Juzeliūnas, E., 2014. Sputter-deposited Mg–Al–Zn–Cr alloys–Electrochemical characterization of single films and multilayer protection of AZ31 magnesium alloy. Corrosion Science 80, 487-493.

Sumitomo, T., Caceres, C., Veidt, M., 2002. The elastic modulus of cast Mg–Al–Zn alloys. Journal of Light Metals 2, 49-56.

Sun, Y., Zhang, B., Wang, Y., Geng, L., Jiao, X., 2012. Preparation and characterization of a new biomedical Mg–Zn–Ca alloy. Materials & Design 34, 58-64.

Swab, J.J., Yu, J., Gamble, R., Kilczewski, S., 2011. Analysis of the diametral compression method for determining the tensile strength of transparent magnesium aluminate spinel. International Journal of Fracture 172, 187-192.

Tan, L., Yu, X., Wan, P., Yang, K., 2013. Biodegradable materials for bone repairs: A review. Journal of Materials Science & Technology 29, 503-513.

Virtanen, S., 2012. Biodegradable Mg Alloys: Corrosion, Surface Modification, and Biocompatibility, Biomedical Applications. Springer, pp. 101-125.

Wang, C.-J., Huang, C.-Y., 2008. Effect of TiO2 addition on the sintering behavior, hardness and fracture toughness of an ultrafine alumina. Materials Science and Engineering: A 492, 306-310.

Wen, C., Mabuchi, M., Yamada, Y., Shimojima, K., Chino, Y., Asahina, T., 2001. Processing of biocompatible porous Ti and Mg. Scripta Materialia 45, 1147-1153.

Wen, C., Yamada, Y., Shimojima, K., Chino, Y., Hosokawa, H., Mabuchi, M., 2004. Compressibility of porous magnesium foam: dependency on porosity and pore size. Materials Letters 58, 357-360.

Willbold, E., Kaya, A., Kaya, R., Beckmann, F., Witte, F., 2011. Corrosion of magnesium alloy AZ31 screws is dependent on the implantation site. Materials Science and Engineering: B 176, 1835-1840.

Willumeit, R., Fischer, J., Feyerabend, F., Hort, N., Bismayer, U., Heidrich, S., Mihailova, B., 2011. Chemical surface alteration of biodegradable magnesium exposed to corrosion media. Acta Biomaterialia 7, 2704-2715.

Witte, F., 2010. The history of biodegradable magnesium implants: A review. Acta Biomaterialia 6, 1680-1692.

Witte, F., Fischer, J., Nellesen, J., Vogt, C., Vogt, J., Donath, T., Beckmann, F., 2010. In vivo corrosion and corrosion protection of magnesium alloy LAE442. Acta Biomaterialia 6, 1792-1799.

Witte, F., Kaese, V., Haferkamp, H., Switzer, E., Meyer-Lindenberg, A., Wirth, C., Windhagen, H., 2005. In vivo corrosion of four magnesium alloys and the associated bone response. Biomaterials 26, 3557-3563.

Witte, F., Ulrich, H., Rudert, M., Willbold, E., 2007. Biodegradable magnesium scaffolds: Part 1: appropriate inflammatory response. Journal of Biomedical Materials Research Part A 81, 748-756.

Wolla, D.W., Davidson, M., Khanra, A., 2015. Constitutive modeling of powder metallurgy processed Al–4% Cu preforms during compression at elevated temperature. Materials & Design 65, 83-93.

Wong, H.M., Yeung, K.W., Lam, K.O., Tam, V., Chu, P.K., Luk, K.D., Cheung, K., 2010. A biodegradable polymer-based coating to control the performance of magnesium alloy orthopaedic implants. Biomaterials 31, 2084-2096.

Wu, S., Liu, X., Yeung, K.W., Guo, H., Li, P., Hu, T., Chung, C.Y., Chu, P.K., 2013. Surface nano-architectures and their effects on the mechanical properties and corrosion behavior of Ti-based orthopedic implants. Surface and Coatings Technology 233, 13-26.

Wu, Y., Kim, G.-Y., 2011. Compaction behavior of Al061 powder in the semi-solid state. Powder Technology 214, 252-258.

Xia, X., Chen, X., Zhang, Z., Chen, X., Zhao, W., Liao, B., Hur, B., 2013. Effects of porosity and pore size on the compressive properties of closed-cell Mg alloy foam. Journal of Magnesium and Alloys 1, 330-335.

Xiao, X., Yu, H., Zhu, Q., Li, G., Qu, Y., Gu, R., 2013. In vivo Corrosion resistance of Ca-P coating on AZ60 magnesium alloy. Journal of Bionic Engineering 10, 156-161.

Xie, W., Liu, Y., Li, D.S., Zhang, J., Zhang, Z.W., Bi, J., 2007. Influence of sintering routes to the mechanical properties of magnesium alloy and its composites produced by PM technique. Journal of Alloys and Compounds 431, 162-166.

Xu, J., Shirooyeh, M., Wongsa-Ngam, J., Shan, D., Guo, B., Langdon, T.G., 2013. Hardness homogeneity and micro-tensile behavior in a magnesium AZ31 alloy processed by equal-channel angular pressing. Materials Science and Engineering: A 586, 108-114.

Xu, L., Pan, F., Yu, G., Yang, L., Zhang, E., Yang, K., 2009. In vitro and in vivo evaluation of the surface bioactivity of a calcium phosphate coated magnesium alloy. Biomaterials 30, 1512-1523.

Yan, X., Hu, L.-x., Yu, S., 2014. Dynamic recrystallization kinetics of as-cast AZ91D alloy. Transactions of Nonferrous Metals Society of China 24, 1683-1689.

Yang, C., Ni, S., Liu, Y., Song, M., 2015. Effects of sintering parameters on the hardness and microstructures of bulk bimodal titanium. Materials Science and Engineering: A 625, 264-270.

Yang, L., Huang, Y., Peng, Q., Feyerabend, F., Kainer, K.U., Willumeit, R., Hort, N., 2011. Mechanical and corrosion properties of binary Mg–Dy alloys for medical applications. Materials Science and Engineering: B 176, 1827-1834.

Yoshihara, S., Manabe, K.-i., Nishimura, H., 2005. Effect of blank holder force control in deep-drawing process of magnesium alloy sheet. Journal of Materials Processing Technology 170, 579-585.

Zaytsev, D., Panfilov, P., 2014. Deformation behavior of human dentin in liquid nitrogen: A diametral compression test. Materials Science and Engineering: C 42, 48-51.

Zhang, E., Yin, D., Xu, L., Yang, L., Yang, K., 2009. Microstructure, mechanical and corrosion properties and biocompatibility of Mg–Zn–Mn alloys for biomedical application. Materials Science and Engineering: C 29, 987-993.

Zhang, J., Dai, C., Wen, Z., Wei, J., 2015. Study on the effect of the coating thickness on corrosion behavior of AZ91D magnesium alloy in m-SBF. International Journal of Electrochemical Science 10, 6002-6013.

Zhang, L.-N., Hou, Z.-T., Ye, X., Xu, Z.-B., Bai, X.-L., Shang, P., 2013a. The effect of selected alloying element additions on properties of Mg-based alloy as bioimplants: A literature review. Frontiers of Materials Science 7, 227-236.

Zhang, X., Li, X., Li, J., Sun, X., 2013b. Processing, microstructure and mechanical properties of biomedical magnesium with a specific two-layer structure. Progress in Natural Science: Materials International 23, 183-189.

Zhang, X., Yuan, G., Niu, J., Fu, P., Ding, W., 2012. Microstructure, mechanical properties, biocorrosion behavior, and cytotoxicity of as-extruded Mg–Nd–Zn–Zr

alloy with different extrusion ratios. Journal of the Mechanical Behavior of Biomedical Materials 9, 153-162.